The FAK–Arp2/3 interaction promotes leading edge advance and haptosensing by coupling nascent adhesions to lamellipodia actin

Vinay Swaminathan, R. S. Fischer, and Clare M. Waterman*
Cell Biology and Physiology Center, National Heart, Lung and Blood Institute, National Institutes of Health, Bethesda, MD 20892-8019

ABSTRACT **Cell migration is initiated in response to biochemical or physical cues in the environment that promote actin-mediated lamellipodial protrusion followed by the formation of nascent integrin adhesions (NAs) within the protrusion to drive leading edge advance. Although FAK is known to be required for cell migration through effects on focal adhesions, its role in NA formation and lamellipodial dynamics is unclear. Live-cell microscopy of FAK$^{-/-}$ cells with expression of phosphorylation deficient or a FERM-domain mutant deficient in Arp2/3 binding revealed a requirement for FAK in promoting the dense formation, transient stabilization, and timely turnover of NA within lamellipodia to couple actin-driven protrusion to adhesion and advance of the leading edge. Phosphorylation on Y397 of FAK promotes dense NA formation but is dispensable for transient NA stabilization and leading edge advance. In contrast, transient NA stabilization and advance of the cell edge requires FAK–Arp2/3 interaction, which promotes Arp2/3 localization to NA and reduces FAK activity. Haptosensing of extracellular matrix (ECM) concentration during migration requires the interaction between FAK and Arp2/3, whereas FAK phosphorylation modulates mechanosensing of ECM stiffness during spreading. Taken together, our results show that mechanistically separable functions of FAK in NA are required for cells to distinguish distinct properties of their environment during migration.**

Monitoring Editor
Yu-Li Wang
Carnegie Mellon University

Received: Aug 21, 2015
Revised: Jan 12, 2016
Accepted: Jan 22, 2016

INTRODUCTION

Directed cell migration occurs during development, the immune response, wound healing, and cancer metastasis. Cells are induced to migrate in response to diffusible cues such as growth factors, haptic cues in the extracellular matrix (ECM), and mechanical cues such as tissue stiffness. Sensing of these cues in the microenvironment stimulates cell polarization and formation of a leading edge protrusion that must adhere to the ECM to allow traction generation, followed by de-adhesion of the cell rear to permit cell advance. Although generally considered as discrete events (Lauffenburger and Horwitz, 1996; Ridley *et al.*, 2003), leading edge protrusion and ECM adhesion are actually tightly coupled both spatially and temporally (Giannone *et al.*, 2004; Gupton and Waterman-Storer, 2006; Schneider *et al.*, 2009). Protrusion occurs via a lamellipodium, which is a narrow (~2 μm), thin (200 nm) projection of the plasma membrane that extends along the cell edge driven by actin cytoskeleton assembly (Pollard and Borisy, 2003). Concurrent with establishment of the lamellipodium is the formation of nascent integrin-mediated adhesions (NAs) that couple the protrusion to ECM binding (Choi *et al.*, 2008). Lamellipodial protrusion and adhesion are believed to be coregulated by complex networks of feedforward and feedback signaling mechanisms (Mitra *et al.*, 2005; Gupton and Waterman-Storer, 2006; Machacek *et al.*, 2009). However, the proteins mediating the physical linkage between the actin cytoskeleton and NAs and the mechanism of their temporal coregulation in lamellipodia are not known.

The dynamics of actin cytoskeletal assembly that drive lamellipodial protrusion has been well studied (Pollard and Borisy, 2003). The

This article was published online ahead of print in MBoC in Press (http://www.molbiolcell.org/cgi/doi/10.1091/mbc.E15-08-0590) on February 3, 2016.

*Address correspondence to: Clare M. Waterman (watermancm@nhlbi.nih.gov).

Abbreviations used: Arp2/3, actin-related protein 2/3; BSA, bovine serum albumin; CB, cytoskeleton buffer; DIC, differential interference contrast; ECM, extracellular matrix; eGFP, enhanced green fluorescent protein; EGTA, ethylene glycol tetraacetic acid; FA, focal adhesions; FAK, focal adhesion kinase; FERM, 4.1, ezrin, radixin, moesin; FN, fibronectin; FSM, fluorescent speckle microscopy; GEF, guanine nucleotide exchange factors; KO, knockout; MEF, mouse embryonic fibroblast; NA, nascent adhesions; NPF, nucleation promoting factor; PIP2, phosphatidylinositol 4,5-bisphosphate; TBS, Tris-buffered saline; TBS-T, Tris-buffered saline-Tween; TIRF, total internal reflection fluorescence; WT, wild type.

lamellipodium comprises a dense actin filament array whose formation is mediated by the Arp2/3 complex (Pollard and Borisy, 2003). Arp2/3 is activated by leading edge, membrane-associated nucleation-promoting factors (NPFs; Higgs and Pollard, 2001), which induce Arp2/3 to bind to the sides of actin filaments to nucleate a polarized, dendritic filament network (Mullins *et al.*, 1998). Rapid polymerization of network-associated filaments toward the cell edge pushes against the plasma membrane, which can drive the assembled actin network backward in a process termed *retrograde flow* (Welch *et al.*, 1997). As new actin continues to assemble at the cell edge, the older actin that has been pushed back from the leading edge mostly depolymerizes within 1–2 min or reorganizes into actin bundles to form the lamella (Ponti *et al.*, 2004; Burnette *et al.*, 2011). This process of polymerization at the front and depolymerization at the rear of lamellipodia results in a *treadmilling* filament array (Pollard and Borisy, 2003). However, if the treadmilling actin network becomes physically coupled to the ECM behind the leading edge, the force of actin polymerization can be used to drive protrusion of the leading edge (Welch *et al.*, 1997).

The physical coupling of the lamellipodial actin network to the ECM is provided by NAs. NAs containing α5β1 integrins (Choi *et al.*, 2011; Bachir *et al.*, 2014) appear as diffraction-limited punctae just behind the leading edge and continue to form at the same rate as leading edge protrusion (Choi *et al.*, 2008). The mechanism of NA nucleation is unknown, although evidence indicates that it requires Arp2/3-mediated actin polymerization (Alexandrova *et al.*, 2008) and that NA proteins may associate as preformed complexes in the cytoplasm before association with ECM-bound integrins (Bachir *et al.*, 2014; Hoffmann *et al.*, 2014). Once formed, only a small fraction of NA elongate and mature into focal adhesions (FAs), whereas the bulk of NAs turn over and disassemble within about 1 min (Choi *et al.*, 2008; Thievessen *et al.*, 2013). NA maturation into FA is dependent on myosin II and formin-mediated actin polymerization (Choi *et al.*, 2008; Iskratsch *et al.*, 2013), whereas turnover of NAs is coincident with actin disassembly at the junction between the lamellipodium and the lamella (Thievessen *et al.*, 2013). Thus NAs and actin filaments exhibit precise spatially and temporally coordinated assembly/disassembly cycles in protruding lamellipodia, thereby coupling actin polymerization to ECM adhesion and preventing leading edge retraction. However, the molecular mechanisms mediating this spatiotemporal coordination or the physical coupling of ECM-bound integrins to actin in NA are unknown.

Focal adhesion kinase (FAK) is a nonreceptor tyrosine kinase that localizes to NAs and mature FAs and is known to regulate cell migration (Mitra *et al.*, 2005; Schaller, 2010). One well-known function of FAK in migration is in promoting the disassembly of mature FAs, as fibroblasts lacking FAK display large, stable FAs (Ilić *et al.*, 1995; Webb *et al.*, 2004; Ezratty *et al.*, 2005; Chan *et al.*, 2010). In addition, FAK activity is required for cell spreading on ECM (Tilghman *et al.*, 2005; Owen *et al.*, 2007), suggesting a role in cell protrusion. Indeed, evidence suggests a possible role for FAK in NAs and regulation of lamellipodial actin. FAK and the adapter protein paxillin localize in early NAs (Choi *et al.*, 2011), where FAK recruits talin, a critical actin- and integrin-binding protein (Lawson *et al.*, 2012). Furthermore, FAK has been shown to directly interact with the Arp3 subunit of the Arp2/3 complex (Serrels *et al.*, 2007), as well as other lamellipodial proteins, including cortactin (Tomar *et al.*, 2012) and the NPF N-WASP (Wu *et al.*, 2004). Thus we hypothesized that FAK in NAs could physically or spatiotemporally couple lamellipodial actin dynamics to ECM adhesion through its interaction with the Arp2/3 complex.

Here we report on the roles of FAK interactions and activity in lamellipodial protrusion and NA dynamics and the consequence of these roles in ECM-dependent cell functions. We show that FAK promotes NA assembly and timely turnover to couple lamellipodial protrusion to adhesions for efficient advance of the leading edge. Using a FERM-domain point mutant previously shown to inhibit Arp2/3 binding to FAK as well as a nonphosphorylatable mutant or a small-molecule inhibitor of FAK kinase activity, we find that local and precisely timed regulation of FAK activity mediates the spatiotemporal coordination and the physical coupling of lamellipodial actin with NAs. Finally, we find mechanistically distinct roles for FAK in cell functions, with Y397 phosphorylation of FAK mediating ECM stiffness sensing, and its interaction with the Arp2/3 complex required for haptosensing.

RESULTS

FAK promotes efficient lamellipodial protrusion and advance of the leading edge

We sought to test the role of FAK in mediating the coupling of lamellipodial protrusion to ECM adhesion through NAs. We thus first examined the requirement for FAK in lamellipodial dynamics. $FAK^{+/+}$ (control) and $FAK^{-/-}$ (FAK-KO) fibroblasts (Ilić *et al.*, 1995) were plated on fibronectin (FN; 10 μg/ml)-coated coverslips and imaged at 3- to 5-s intervals by high-resolution differential interference contrast (DIC) microscopy. Time-lapse movies showed that whereas control cells underwent random migration, loss of FAK caused cells to adhere tightly to the ECM and completely inhibited cell migration, as reported (Tilghman *et al.*, 2005; Owen *et al.*, 2007). In addition, examination of lamellipodial cell edges revealed that FAK-KO cells ruffled wildly compared with the edges of control cells that appeared more stably attached to the substrate even as they protruded and retracted (Supplemental Movie S1). Kymographs of lamellipodia showed that both control cells and FAK-KO cells exhibited cycles of protrusion and retraction (Bear *et al.*, 2002; Giannone *et al.*, 2004). However, over the course of a movie, the leading edge of control cells advanced substantially, whereas the ruffling edges of FAK-KO cells did not (Figure 1A).

To determine the precise defect in the protrusion–retraction cycle that caused the lack of leading edge advance in FAK-KO cells, we extracted from kymographs the velocity (V_P or V_R; distance/time) and distance (D_P or $D_{R)}$ of each protrusion or retraction phase (Figure 1, B and C). This analysis showed that loss of FAK significantly increased the velocities and distances of both protrusion and retraction (Figure 1, B and C). In addition, comparison of the protrusion and retraction distances showed that in control cells, protrusions extended significantly farther than retractions, whereas in FAK-KO cells, protrusion and retraction distances were not significantly different (Figure 1C). To quantify how well protrusion overcomes retraction to mediate leading edge advance, we determined the "protrusion efficiency" as the percentage further that the cell edge protruded than it retracted ($(D_P - D_R/D_P) \times 100$; Figure 1D). This showed that for control cells, protrusion efficiency was ~60%, and loss of FAK decreased the protrusion efficiency fourfold. This decrease in protrusion efficiency resulted in a fivefold reduction in net edge advance rate (net protrusion distance/total time of movie) of the leading edge in FAK-KO cells compared with control (Figure 1E). Reexpressing full-length mCherry-tagged FAK (wtFAK) at near-endogenous levels in FAK-KO cells (Supplemental Figure S1A) rescued all defects in protrusion and retraction parameters, restoring them to the same levels observed in control cells. Thus FAK promotes leading edge advance by reducing the distance of retraction relative to that of protrusion.

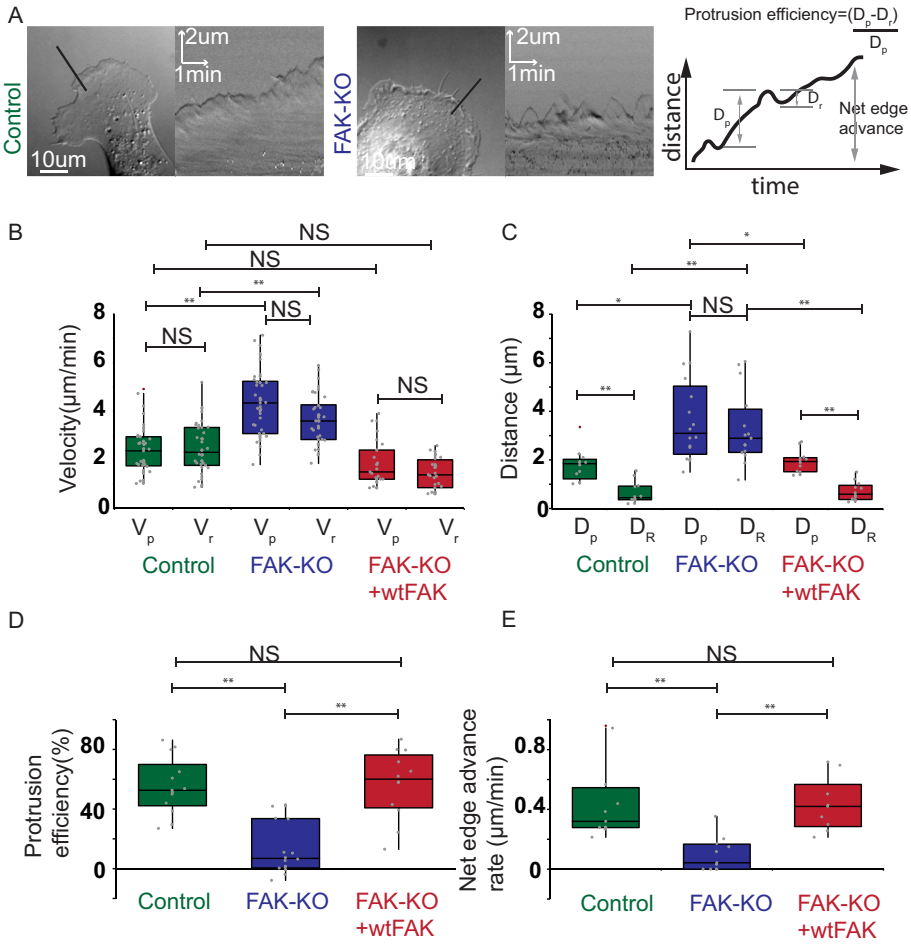

FIGURE 1: FAK promotes efficient lamellipodial protrusion and advance of the leading edge. (A) Left and middle, representative DIC micrographs of FAK$^{+/+}$ (control; left, left) and FAK$^{-/-}$ knockout (FAK-KO; middle, left) MEFs plated on fibronectin-coated coverslips for 4 h and then imaged. Black line indicates line along which the kymograph (right) was obtained. Far right, schematic diagram of a kymograph showing different parameters used for quantifying leading edge dynamics. Scale bars, 10 μm (left), distance 2 μm, time 1 min (right). (B) Box plot of velocities (μm/min) of protrusion (V_p) and retraction (V_r) of control (green), FAK-KO (blue), and FAK-KO expressing mCherry-tagged, wild-type FAK (FAK-KO + wtFAK; red) cells. (C) Box plot of distances (μm) of protrusion (D_p) and retraction (D_r) of control (green), FAK-KO (blue), and FAK-KO + wtFAK (red) cells). (D) Box plot of protrusion efficiency (%) for control (green), FAK-KO (blue) and FAK-KO + wtFAK (red) cells. (E) Box plot of net edge advance (μm /min) of control (green), FAK-KO (blue), and FAK-KO + wtFAK (red) cells (10–12 cells/condition for all the data reported). $^{**}p < 0.0001$, $^{*}p < 0.005$; NS, not significant; Mann–Whitney *U* test.

protrusion, and instead of disassembling, many of them grew into mature FAs or slid centripetally and disassembled (Supplemental Movie S2).

We performed quantitative analysis of time-lapse movies to determine the defect in NA dynamics caused by loss of FAK. We first confirmed that our FAK-KO cells were representative of known functions of FAK in promoting the disassembly of large FAs (Ilić *et al.*, 1995; Webb *et al.*, 2004). Quantification of FA area showed that compared with control, FAK-KO cells had significantly larger FAs, as expected (Figure 2B; Ilić *et al.*, 1995). We then determined the effects of FAK-KO on NAs (Figure 2C-F). We defined NAs as eGFP-paxillin clusters with areas and lifetimes <0.25 μm^2 (Thievessen *et al.*, 2013) and 200 s (Choi *et al.*, 2008), respectively, and FAs as those with greater areas and lifetimes. Kymograph analysis of NA lifetime (Figure 2, A, right, and C) showed that in control cells, NAs had a broad distribution of lifetimes, with two qualitative peaks, one between 0 and 50 s and the other between 90 and 150 s. In contrast, FAK-KO cells showed only a single peak between 0 and 50 s and a complete loss of the longer-lived population of NAs. This resulted in a significantly shorter average lifetime of NAs in FAK-KO cells than in controls (Figure 2D). To test whether FAK was required for nucleation of new NAs or their transition into mature FAs, we measured NA formation density (NAs formed per unit area of lamellipodia; Figure 2E) and maturation fraction (NA matured/NA formed; Figure 2F; Thievessen *et al.*, 2013). We found that, compared with control, FAK-KO exhibited decreased NA formation density and increased NA maturation fraction (Figure 2, E and F). Reexpression of wtFAK in FAK-KO cells restored both FA and NA phenotypes to those observed in control cells, suggesting that these effects are directly due to FAK (Figure 2, C– F). Thus, in addition to its established role in the lamella in limiting FA size (Ilić *et al.*, 1995) and promoting FA disassembly (Webb *et al.*, 2004), our results show that FAK promotes the formation, transient stabilization, and subsequent turnover of NAs in the lamellipodium and inhibits their maturation into FAs in the lamella. Taken together, our results suggest that FAK promotes advance of the leading edge by facilitating formation and properly timed turnover of NAs within the lamellipodium.

FAK couples leading edge protrusion to formation and turnover of NAs in the lamellipodium

The finding that FAK is required to reduce the distance of the retraction phase suggests a role for FAK in coupling leading edge protrusion to substrate adhesion, possibly through formation of NAs. We expressed enhanced green fluorescent protein (eGFP)–paxillin as a marker of NAs (Choi *et al.*, 2008; Thievessen *et al.*, 2013) in control and FAK-KO cells and imaged NA dynamics at 3-s intervals by total internal reflection fluorescence (TIRF) microscopy (Figure 2A). Examination of time-lapse movies showed that in control cells, each round of edge protrusion was accompanied by the formation of a row of tightly spaced NAs all along the cell edge, and the bulk of these NAs disassembled as the next cycle of protrusion ensued and the next row of NAs was formed. In contrast, in FAK-KO cells, protrusions formed with apparently fewer NAs, they were not organized in a row at the edge but instead sparsely distributed throughout the

FAK couples leading edge protrusion to NAs independently of Y397 phosphorylation

To determine the mechanism by which FAK couples lamellipodial protrusion to NAs, we first examined the role of FAK phosphorylation. Autophosphorylation on tyrosine 397 (Y397) mediates relief of autoinhibition and activation of FAK kinase activity and induces its binding to SH2 domain–containing signaling proteins (Frame *et al.*, 2010). We used time-lapse DIC imaging to compare leading edge

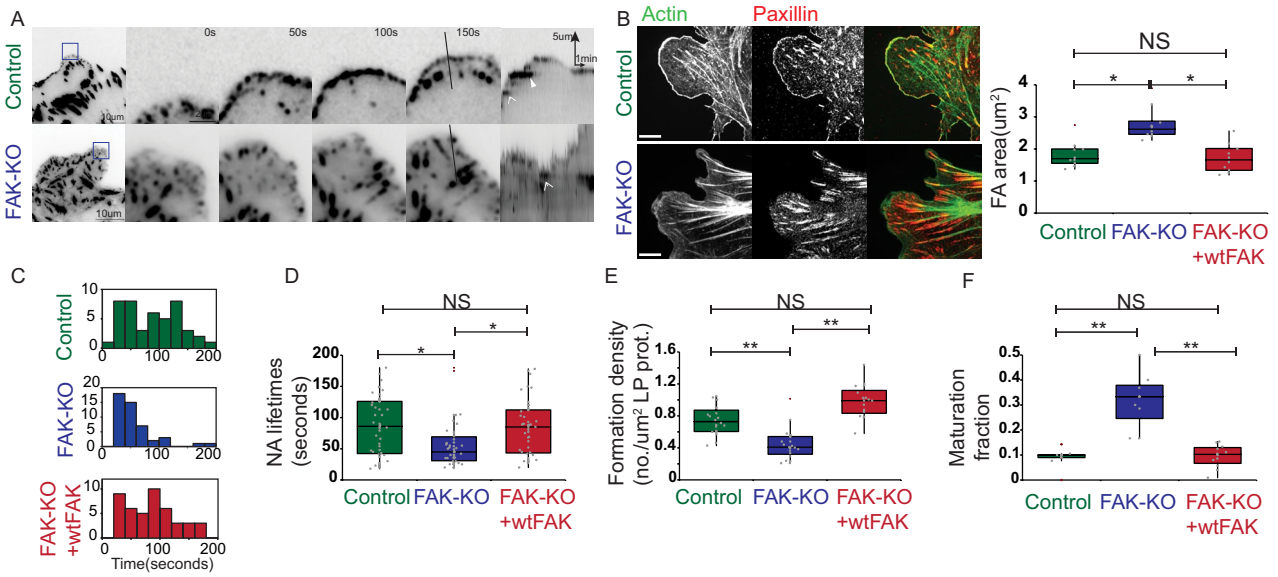

FIGURE 2: FAK couples leading edge protrusion to formation and turnover of NAs in the lamellipodium. (A) Left, representative TIRF micrographs of FAK$^{+/+}$ (control, top) and FAK$^{-/-}$ knockout (FAK-KO, bottom) MEF cells expressing eGFP-paxillin (contrast inverted). Scale bar, 10 μm. Blue box indicates area zoomed in for images to the right, a TIRF time-lapse image sequence of eGFP-paxillin–marked adhesions at the leading edge. Time in seconds. Scale bar, 2 μm. Black line indicates the line along which the kymograph on the far right was obtained. White open arrows show extremely short-lived NAs, and white closed arrows indicate medium and longer-lived NAs. Scale bars, distance 5 μm, time 1 min. (B) Left, representative confocal micrographs of control (top) and FAK-KO (bottom) cells showing Alexa 655–phalloidin staining of actin (green) and immunofluorescence of paxillin (red), along with the color merge. Scale bar, 10 μm. Right, quantification of focal adhesion size (area, μm^2) from analysis of fluorescence images of paxillin in the noted cells (10 cells/condition). Color coding in B (right) and C– F: control (green), FAK-KO (blue), and FAK-KO expressing mCherry tagged wild-type FAK (FAK-KO + wtFAK; red). (C) Distribution of the lifetimes of eGFP-paxillin–marked NA in control (top), FAK-KO (middle), and FAK-KO + wtFAK (bottom) cells. Bin size, 20 s; 50–70 NAs in five or six cells/condition. (D) Box plots of quantification of NA lifetimes from distributions in C. (E) Box plot of NA formation density (number/μm^2 lamellipodia protrusion area) marked by eGFP-paxillin in protruding lamellipodia of control, FAK-KO, and FAK-KO + wtFAK cells (17–20 protrusions, five or six cells/condition). (F) Box plot of maturation fraction (dimensionless, NAs formed − NAs disassembled/NAs that mature) among >100 NAs in protruding lamellipodia of control, FAK-KO, and FAK-KO + wtFAK cells (10–12 protrusions, five cells/condition). $^{**}p < 0.0001$, $^{*}p < 0.005$; NS, not significant; Mann–Whitney *U* test.

dynamics of FAK-KO cells with FAK-KO cells expressing GFP fusions of either wt*FAK* or nonphosphorylatable FAK (*FAK*^{Y397F}) at near-endogenous levels (Supplemental Figure S1A and Supplemental Movie S4). Quantitative analysis of kymographs showed that expression of either wt*FAK* or *FAK*^{Y397F} in FAK-KO cells rescued the increased edge protrusion and retraction velocities and distances that were induced by loss of FAK (Figure 3, B and C). Furthermore, expression of either wtFAK or *FAK*^{Y397F} in FAK-KO cells was sufficient to increase both the protrusion efficiency and net edge advance compared with FAK-KO (Figure 3, D and E) and restore it to levels similar to those in control cells (Figure 1, D and E). These results show that FAK is required to promote protrusion efficiency and net edge advance independently of Y397 phosphorylation.

We next tested whether Y397 phosphorylation was required for FAK function in NA formation and turnover. We expressed wtFAK or FAK^{Y397F} in FAK-KO cells and quantified NA dynamics in time-lapse TIRF movies (Figure 3F and Supplemental Movie S3). We first verified that both eGFP-FAK and eGFP-FAK^{Y397F} could be used as markers for NA dynamics by confirming their colocalization with mCherry-paxillin in NAs and mature FAs. We also verified that FAK phosphorylation on Y397 was required for inhibiting the formation of large FAs, as previously reported (Supplemental Figure S1D; Webb *et al.*, 2004; Hamadi *et al.*, 2005). We then performed kymograph analysis of NA lifetimes (Figure 3F) in FAK-KO cells expressing either wtFAK or *FAK*^{Y397F}. This showed that *FAK*^{Y397F} was sufficient to rescue the reduction in average lifetime of NA induced by loss of FAK and restore it to levels similar to that in controls or FAK-KO cells reconstituted with wtFAK (Figures 3H and 2D). However, examination of the distribution of NA lifetimes showed that the increase in average lifetime in FAK-KO cells expressing *FAK*^{Y397F} relative to FAK-KO resulted specifically from an increase in the population of longer-lived NAs (~90–200 s; Figure 3G) and a loss of the shorter-lived population, suggesting a role for Y397 phosphorylation in promoting rapid turnover of NA. Analysis of the NA maturation fraction showed that expression of *FAK*^{Y397F} in FAK-KO cells rescued the increase in NA maturation induced by loss of FAK (Figure 3I). Analysis of NA formation density showed that whereas expression of wtFAK in FAK-KO cells increased NA density relative to that in FAK-KO cells and similar to the level observed in controls (Figure 2E), expression of *FAK*^{Y397F} in FAK-KO did not (Figure 3J). These results show that Y397 phosphorylation of FAK is required for dense NA formation and rapid NA turnover in lamellipodia. Further, since Y397 phosphorylation is not required for efficient protrusion (Figure 3D), this suggests that neither high NA formation density nor rapid NA turnover is critical to leading edge advance.

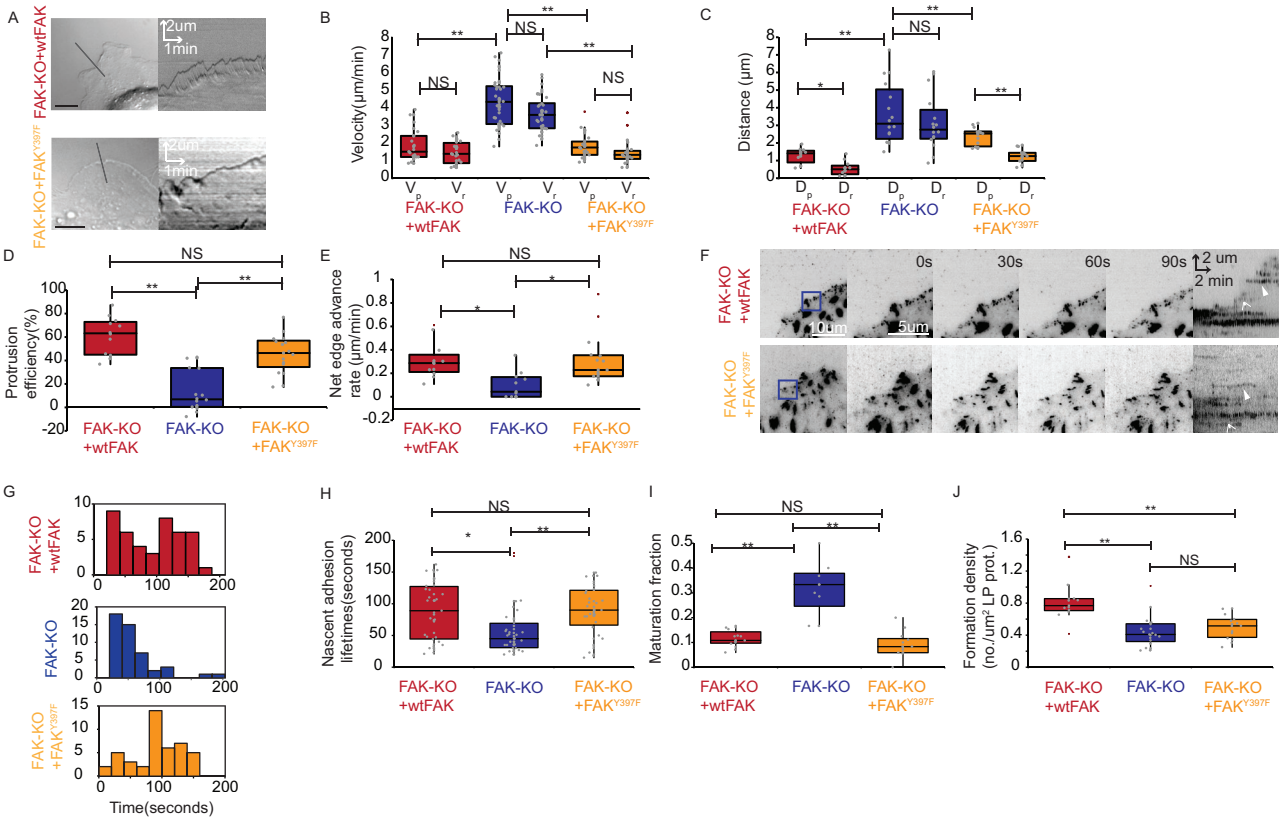

FIGURE 3: FAK couples leading edge protrusion to NAs independent of Y397 phosphorylation. (A) Left, representative DIC micrographs of FAK$^{-/-}$ knockout (FAK-KO) MEFs expressing eGFP-tagged wild-type (FAK-KO + wtFAK; top) and FAK-KO cells expressing eGFP-tagged FAK^{Y397F} mutant (FAK-KO + FAK^{Y397F}; bottom). Cells were imaged 4–6 h after plating on 10 μg/ml fibronectin–coated coverslips. Black line indicates the line along which the kymograph on the right was obtained. Scale bars, 10 μm (left), distance 2 μm, time 1 min (right). (B) Box plot of velocities (μm/min) of protrusion (V_p) and retraction (V_r) of FAK-KO cells expressing the noted FAK constructs. Color coding in B–J: FAK-KO + wtFAK (red), FAK-KO (blue), and FAK-KO + FAK^{Y397F} (yellow) cells. (C) Box plot of distances (μm) of protrusion (D_p) and retraction (D_r) of FAK-KO cells expressing the noted FAK constructs. (D) Box plot of protrusion efficiency (%) of FAK-KO + wtFAK, FAK-KO, and FAK-KO + FAK^{Y397F} cells. (E) Box plot of net edge advance (μm/min) of FAK-KO + wtFAK, FAK-KO, and FAK-KO + FAK^{Y397F} cells (10–12 cells/condition). **$p < 0.0001$, *$p < 0.005$; NS, not significant; Mann–Whitney *U* test. (F) Left, representative TIRF micrographs of FAK-KO cells expressing either EGFP-wtFAK (top) or EGFP-FAK^{Y397F} (bottom; scale bar, 10 μm). Contrast inverted. Blue box indicates area zoomed in for right images, a TIRF time-lapse image sequence of eGFP-FAK (top)– or eGFP-FAK^{Y397F} (bottom)–marked adhesions at the leading edge. Time in seconds. Scale bar, 5 μm. Far right, kymograph analysis of NA dynamics from preceding images. White open arrowheads, extremely short-lived NA; white closed arrowheads, longer-lived NA. Scale bars, distance 2 μm, time 2 min. (G) Distribution of NA lifetimes in FAK-KO cells expressing either eGFP-wtFAK (FAK-KO + wtFAK; top) or EGFP-FAK^{Y397F} (FAK-K + FAK^{Y397F}; bottom). Middle, distribution of *EGFP*-paxillin–marked NA in FAK-KO cells (50–70 NAs in five or six cells/condition). (H) Box plots of quantification of NA lifetimes (seconds) from distributions in G. (I) Box plot for maturation fraction (dimensionless, NAs formed/NAs that mature) among >100 NAs in protruding lamellipodia of FAK-KO + EGFP-FAK, FAK-KO, and FAK-KO + EGFPFAK^{Y397F} cells (10–12 protrusions, five cells/condition). (J) Box plot of NA formation density (number/μm^2 lamellipodia protrusion area) in protruding lamellipodia marked by eGFP-FAK in FAK-KO + FAK cells, eGFP-paxillin in FAK-KO cells or EGFP-FAK^{Y397F} in FAK-KO + FAK^{Y397F} cells (17–20 protrusions, five or six cells per condition). **$p < 0.0001$, *$p < 0.005$; NS, not significant; Mann–Whitney *U* test. Note: FAK-KO data in all plots are the same data as presented in Figure 1.

FAK–Arp2/3 interaction promotesArp2/3 localization to NAs to mediate efficient protrusion and leading edge advance

The Arp2/3 complex promotes lamellipodial actin polymerization and has been shown to bind directly to FAK both in cells and in vitro (Serrels *et al.*, 2007). We thus hypothesized that the interaction of FAK with Arp2/3 might couple NA formation or turnover to leading edge protrusion. To test this, we introduced point mutations in the FERM domain of mCherry- or eGFP-tagged FAK (*FAK^{K38AR86A}*), which have been shown to disrupt its interaction with the Arp3 subunit of the Arp2/3 complex (Serrels *et al.*, 2007), and analyzed its localization and effects on protrusion and adhesion dynamics.

We first examined the effect of FAK phosphorylation and the effect of the FERM-domain mutant on the localizations of FAK and Arp2/3 in lamellipodia. Immunofluorescence localization of endogenous ArpC2 subunit of the Arp2/3 complex in FAK-KO cells reconstituted with fluorescence-tagged FAK mutants expressed at near-endogenous levels (Supplemental Figure S1A) showed that Arp2/3, wtFAK, *FAK^{Y397F}*, and *FAK^{K38AR86A}* all localized in punctate distributions in thin bands along the leading edge of lamellipodia.

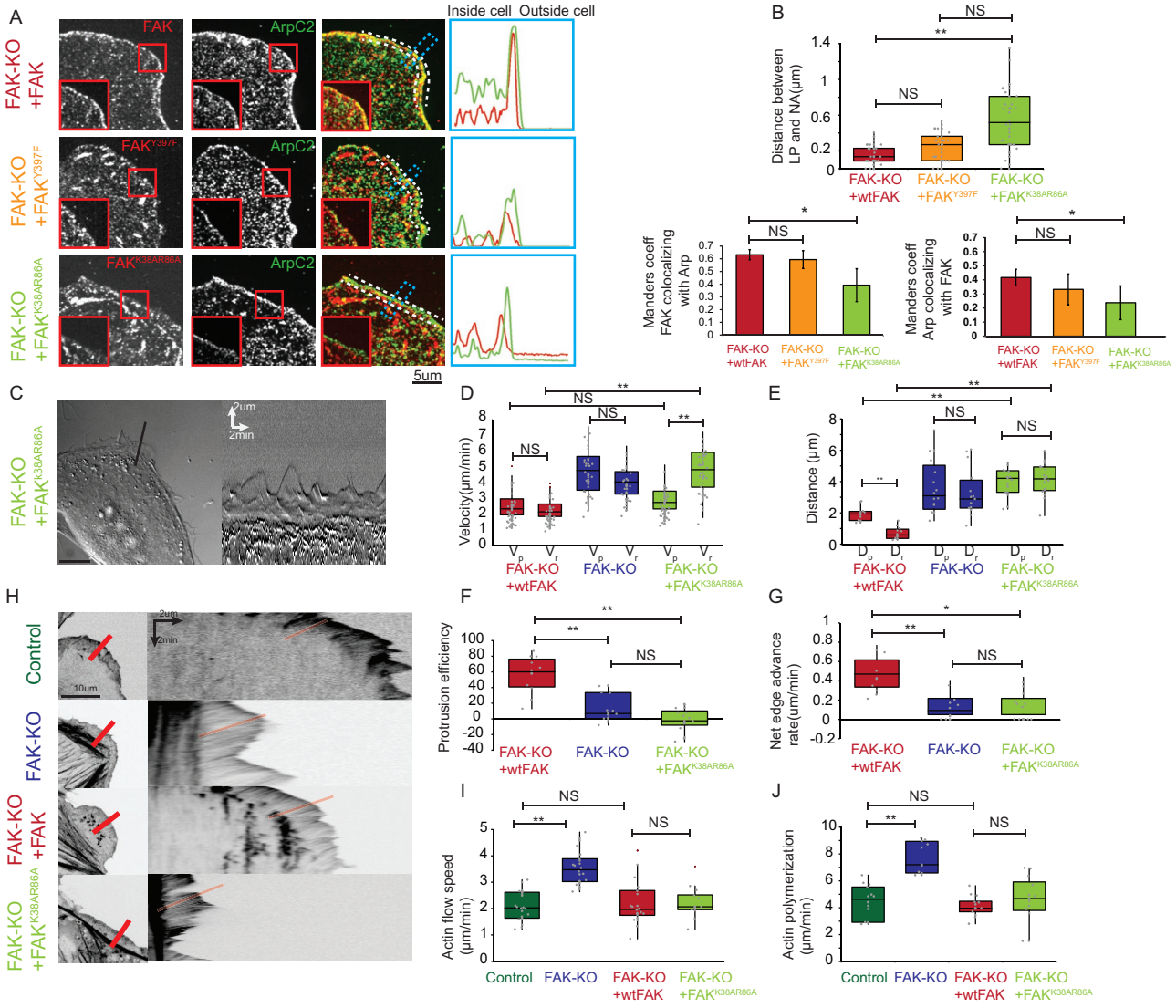

FIGURE 4: FAK–Arp2/3 interaction promotes recruitment of Arp2/3 to NA to mediate efficient protrusion and leading edge advance. (A) Left, representative confocal micrographs of FAK$^{-/-}$ knockout (FAK-KO) MEF cells transfected with mCherry-tagged wild-type FAK (FAK-KO + wtFAK; top), eGFP-tagged FAK^{Y397F} mutant (FAK-KO + FAK^{Y397F}; middle) or mCherry tagged FAK^{K38AR86A} mutant (FAK-KO + FAK^{K38AR86A}; bottom), showing respective *FAK* channel in red and immunostaining for ArpC2 subunit of the Arp2/3 complex (green), with color overlay. Zoom of the red box is shown in the inset of each channel. Blue box indicates the position of the line scan used for quantification of fluorescence intensities in right panel and B, top. White box indicates the position of the line scan used for quantification of colocalization coefficients in B, bottom left and bottom right. Scale bar, 5 μm. Right, representative line scans of fluorescence intensities of mCherry-FAK or mCherry FAK^{K38AR86A} (top and bottom; red) or EGFP- FAK^{Y397F} (middle; red) and intensity of immunostained ArpC2 subunit of Arp2/3 complex (green). (B) Top, box plot of distance between the peak of fluorescence intensity of line scans of the ArpC2 subunit of Arp2/3 complex immunostaining to the peak of fluorescence intensity of line scans of the indicated expressed FAK mutant, FAK-KO + wtFAK (red), FAK-KO + FAK^{Y397F} (yellow), and FAK-KO + FAK^{K38AR86A} (light green; 38 protrusions/condition, five to seven cells/condition). Bottom left, bar plot of the Manders coefficient of colocalization for indicated expressed FAK constructs with immunostained ArpC2 subunit of the Arp2/3 complex, FAK-KO + wtFAK (red), FAK-KO + FAK^{Y397F} (yellow), and FAK-KO + FAK^{K38AR86A} (light green). Bottom right, bar plot of the Manders coefficient of colocalization for immunostained ArpC2 subunit for the Arp2/3 complex with indicated expressed FAK construct. Error bars indicate SD (five cells/condition). $^{**}p < 0.0001$, $^{*}p < 0.005$; NS, not significant; Mann–Whitney *U* test. (C) Representative DIC micrograph of FAK-KO MEFs expressing mCherry-tagged FAK^{K38AR86A} imaged 4 h after plating on fibronectin-coated coverslips. Black line indicates the line along which the kymograph on the right was obtained. Scale bars, 10 μm (left), distance 2 μm, time 2 min (right). (D) Box plot of velocities (μm/min) of protrusion (V_p) and retraction (V_r) of FAK-KO cells expressing the noted FAK construct (10–12 cells/condition). Color coding in D–G, I, J: FAK-KO + wtFAK cells (red), FAK-KO + FAK^{K38AR86A} cells (light green), and FAK-KO cells (blue). (E) Box plot of distances (μm) of protrusion (D_p) and retraction (D_r) of FAK-KO cells expressing the noted FAK construct (10–12 cells/condition). (F) Box plot of protrusion efficiency (%) for FAK-KO + FAK, FAK-KO, and FAK-KO + FAK^{K38AR86A} cells (10–12 cells/condition). (G) Box plot of net edge advance (μm/min) of FAK-KO + FAK, FAK-KO, and FAK-KO + FAK^{K38AR86A} cells (10–12 cells/condition). $^{**}p < 0.0001$, $^{*}p < 0.005$; NS, not significant;

Examination of color overlay images of Arp2/3 together with either wtFAK or *FAK*^{Y397F} in FAK-KO cells showed that a subset of Arp2/3 puncta partially colocalized with FAK-containing NAs in spite of the reduced NA density in cells containing *FAK*^{Y397F} (Figure 4, A and B). In addition, in cells reconstituted with wtFAK, line scan analysis showed that FAK and Arp2/3 exhibited indistinguishable peaks of localization at the leading edge, whereas in cells reconstituted with *FAK*^{Y397F}, Arp2/3 exhibited two peaks near the leading edge, with *FAK*^{Y397F} colocalizing with the proximal peak. In addition, Manders analysis of lamellipodia showed that both wtFAK and *FAK*^{Y397F} exhibited a high degree of colocalization (Figure 4B). In contrast, in FAK-KO cells reconstituted with *FAK*^{K38AR86A}, although Arp2/3 remained localized along the leading edge and *FAK*^{K38AR86A} localized to NAs, color overlay images showed a reduction in colocalization of Arp2/3 and *FAK*^{K38AR86A}, line scans showed that the peak of *FAK*^{K38AR86A} was displaced just proximal to the peak of Arp2/3 at the leading edge, and a Manders colocalization analysis revealed a significant reduction in *FAK*^{K38AR86A}–Arp2/3 colocation (Figure 4B). These results suggest that the FAK–Arp2/3 interaction promotes localization of Arp2/3 to NAs, and yet Arp2/3 targets to lamellipodia and FAK targets to NAs independent of their interaction with each other.

We then assessed the role of the FAK–Arp2/3 interaction in lamellipodial protrusion dynamics by DIC microscopy (Supplemental Movie S4). Examination of movies and kymographs of the leading edge showed that, like FAK-KO cells (Figure 1A), FAK-KO cells reconstituted with *FAK*^{K38AR86A} appeared to exhibit extensive ruffling and did not advance their leading edges (Figure 4C). Quantitative analysis of kymographs confirmed this. Measurement of the velocity and distance of protrusion and retraction phases showed that whereas expression of wt*FAK* in FAK-KO cells rescued the increased edge velocities and distances induced by loss of FAK, expression of *FAK*^{K38AR86A} in FAK-KO selectively reduced the velocity of protrusion but did not rescue either the velocity of retraction or the distances of protrusion or retraction (Figure 4, D and E). Furthermore, expression of *FAK*^{K38AR86A} in FAK-KO cells was not sufficient to restore defects in either the protrusion efficiency or net edge advance induced by FAK-KO (Figure 4, F and G). These results suggest that the FAK–Arp2/3 interaction is required for slowing the rate of leading edge protrusion and reducing the distance of cell-edge retraction to stabilize lamellipodia and promote advance of the leading edge.

Previous work using in vitro assays suggested that FAK binding mildly enhances the actin polymerization activity of Arp2/3 (Serrels *et al.*, 2007), suggesting that the lamellipodial defects seen in *FAK*^{K38AR86A} could be due to effects on lamellipodial actin assembly. To test this prediction in cells, we expressed GFP-actin at low levels and performed time-lapse fluorescence speckle microscopy (FSM) using a spinning-disk confocal microscope (Vallotton *et al.*, 2003). Kymographs of FSM movies allowed simultaneous measurement of the rates of leading edge movement and lamellipodial actin retrograde flow (Figure 4H and Supplemental Movie S5). Because actin polymerization contributes to both leading edge protrusion and retrograde actin flow, we estimated the actin polymerization rate as the sum of these two rates (Renkawitz *et al.*, 2009). This analysis surprisingly showed that, compared with control, loss of FAK actually significantly increased the actin polymerization rate in lamellipodia, indicating that FAK may in fact reduce leading edge actin polymerization (Figure 4J). However, expression of either wtFAK or *FAK*^{K38AR86A} in FAK-KO cells restored actin polymerization rates to control levels, indicating that FAK might reduce actin assembly in lamellipodia independently of its interaction with Arp2/3 (Figure 4, I and J). Taken together, these results suggest that the FAK–Arp2/3 interaction is required for recruiting Arp2/3 to NA to inhibit edge retraction to drive efficient protrusion and leading edge advance, but this is independent of FAK's role in regulating lamellipodial actin assembly.

The FAK–Arp2/3 interaction couples leading edge protrusion to the formation and turnover of NA

We next sought to determine the role of the FAK-Arp2/3 interaction in regulating NA dynamics. We first verified that mCherry-tagged *FAK*^{K38AR86A} colocalized with GFP-paxillin in NA and mature FA (Supplemental Figure S1B). Analysis of the FA area showed that expression of *FAK*^{K38AR86A} in FAK-KO cells was sufficient to rescue the induction of large FAs by loss of FAK, indicating that FAK limits FA size independently of its interaction with Arp2/3 (Figure 5, A and B). We then analyzed the effects of *FAK*^{K38AR86A} on NA dynamics (Figure 5C and Supplemental Movie S6). This showed that whereas expression of wtFAK in FAK-KO cells rescued the reduction in NA lifetime induced by loss of FAK, expression of *FAK*^{K38AR86A} in FAK-KO cells did not, with histograms revealing a loss of longer-lived NAs (90–200 s) and an increase in shorter-lived NAs (0–50 s) compared with wtFAK in FAK-KO cells (Figure 5D). This shift in lifetime distribution led to an average reduction in NA lifetimes similar to FAK-KO (Figure 5E). This indicates that the FAK-Arp2/3 interaction increases the lifetime of NAs by promoting their transient stabilization. Analysis of NA formation density and maturation fraction showed that expression of *FAK*^{K38AR86A} in FAK-KO cells failed to restore either NA formation or maturation to the levels observed in FAK-KO cells reconstituted with wtFAK (Figure 5, F and G). These results suggest that the FAK–Arp2/3 interaction promotes dense formation, transient stabilization, and subsequent turnover of NA in the lamellipodium but is dispensable for limiting FA size in the lamella. Together these results support the notion that the FAK–Arp2/3 interaction is required for coupling lamellipodial protrusion to the dense formation and properly timed turnover of NA within the lamellipodium to drive efficient leading edge advance.

Arp2/3 locally inhibits FAK activity to couple lamellipodial protrusion to transient NA stabilization and turnover for efficient leading edge protrusion

Previous work showed that activation of FAK by Y397 phosphorylation disrupts its interaction with the Arp3 subunit of Arp2/3 (Serrels *et al.*, 2007), suggesting the hypothesis that Arp2/3 sequestration of inactive FAK might be critical to coupling lamellipodial protrusion to

Mann–Whitney *U* test. Note: FAK-KO data are the same as in Figure 1. (H) Left, representative inverted-contrast confocal micrographs of eGFP-actin in FAK$^{+/+}$ MEFs expressing eGFP-actin (control, top) and in FAK-KO (second row), FAK-KO + FAK (third row), or FAK-KO + FAK^{K38AR86A} cells (bottom). The red bar indicates the line along which the kymograph (right) of eGFP-actin was done, in which the red line shows an example of a slope of retrograde actin flow used to measure actin flow velocity. (I) Box plot of speed of retrograde actin flow (μm/min) from protrusions in FAK$^{+/+}$ (control, dark green in I and J), FAK-KO, FAK-KO + wtFAK, and FAK-KO + FAK^{K38AR86A} cells (15–23 cells/condition). (J) Box plot of actin polymerization rate (μm/min) calculated as the sum of protrusion rate and retrograde actin flow rate in control, FAK-KO, FAK-KO + wtFAK, and FAK-KO + FAK^{K38AR86A} cells (15–23 cells/ condition).). $^{**}p < 0.0001$, $^{*}p < 0.005$; NS, not significant; Mann–Whitney *U* test.

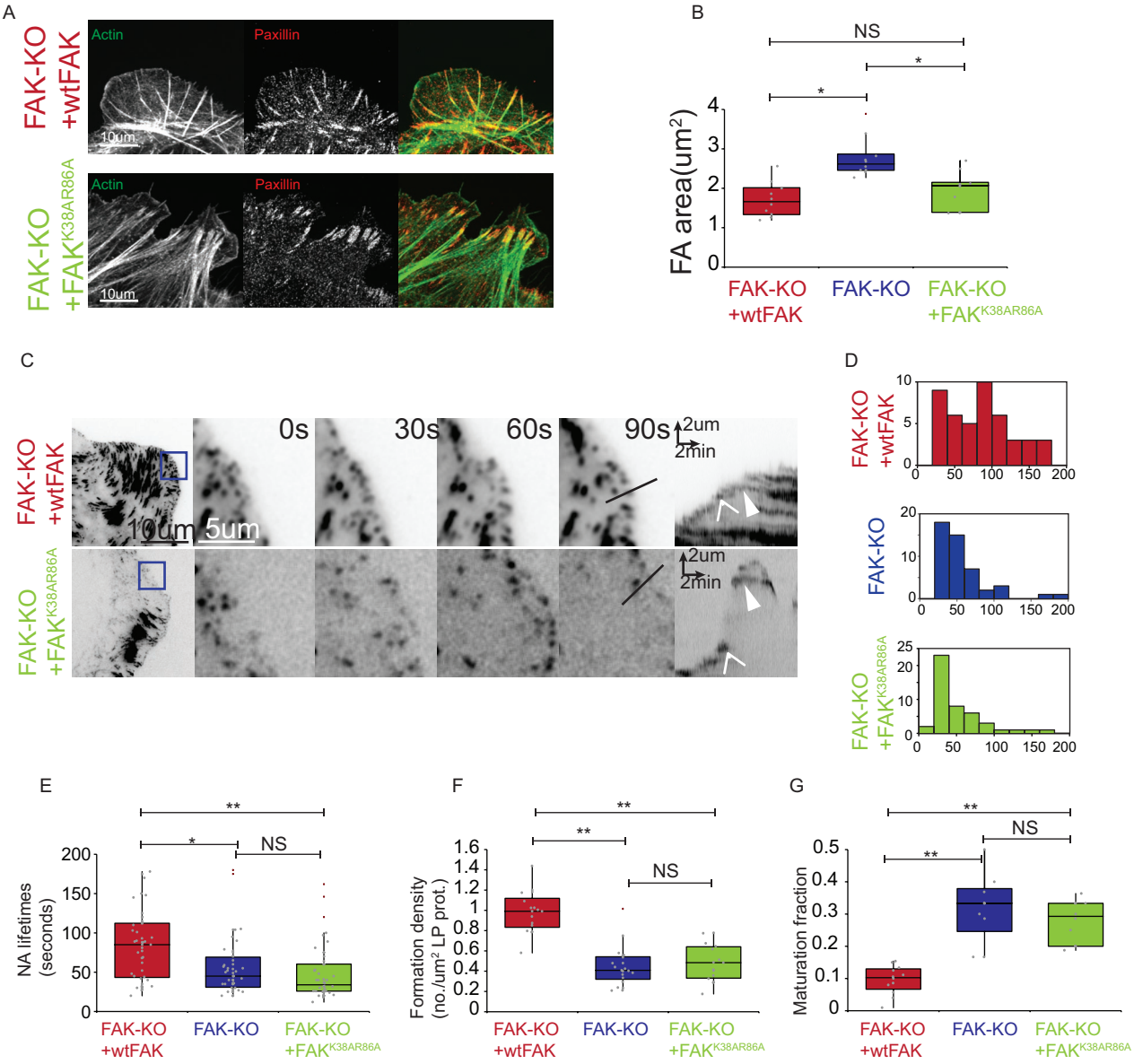

FIGURE 5: The FAK-Arp2/3 interaction couples leading edge protrusion to the formation and turnover of NAs. (A) Left, representative confocal micrographs of FAK$^{-/-}$ (FAK-KO) MEF cells expressing mCherry-tagged wild-type FAK (FAK-KO + wtFAK; top) and/or mCherry-tagged FAK^{K38AR86A} mutant (FAK-KO + FAK^{K38AR86A}; bottom, showing Alexa 655–phalloidin staining of actin (green) and immunofluorescence of Alexa 488–paxillin (red). Scale bar, 10 μm. (B) Quantification of FA size (area, μm^2) from analysis of immunofluorescence images of paxillin in FAK-KO cells expressing the noted FAK construct (10 cells/condition). Color coding in B and D–G: FAK-KO + wtFAK (red), FAK-KO (blue), and FAK-KO + FAK^{K38AR86A} (light green) cells. (C) Left, representative TIRF micrograph of *EGFP*-paxillin in FAK-KO cells expressing EGFP paxillin and either mCherry-wtFAK (top) or mCherry-FAK^{K38AR86A} (contrast inverted). Scale bar, 10 μm. Blue box indicates area zoomed in at right TIRF time-lapse image sequence of eGFP-paxillin in FAK-KO + wtFAK (top)– or FAK-KO + FAK^{K38AR86A} (bottom)–marked adhesions at the leading edge. Time in seconds. Scale bar, 5 μm. Far right, kymograph analysis of NA dynamics. White open arrowheads, extremely short-lived NAs; white closed arrowheads, longer-lived NAs. Scale bar, distance 2 μm, time 2 min. (D) Distribution of lifetimes of eGFP-paxillin–marked NAs in FAK-KO + wtFAK (top), FAK-KO (middle), and FAK-KO + FAK^{K38AR86A} (bottom) cells in 20-s bins (50–70 NAs in five or six cells/condition). (E) Box plots of quantification of NA lifetimes (seconds) from distributions in D. (F) Box plot of NA formation density marked (number/μm^2 lamellipodia protrusion area) by eGFP-paxillin in protruding lamellipodia of FAK-KO + wtFAK, FAK-KO, and FAK-KO + FAK^{K38AR86A} cells (17–20 protrusions, five or six cells per condition)]. (G) Box plot for maturation fraction (dimensionless, NAs formed/NAs that mature) among >100 NAs in protruding lamellipodia of FAK-KO + wtFAK, FAK-KO, and FAK-KO + FAK^{K38AR86A} cells. $^{**}p < 0.0001$, $^{*}p < 0.005$; NS, not significant; Mann–Whitney *U* test. Note: FAK-KO + wtFAK and FAK-KO data in B and J–L are the same as in Figure 2, B and E–G, respectively.

NA formation. To test this, we first sought to determine the role of the FAK–Arp2/3 interaction and Arp2/3 activity in regulation of FAK activation in cells. We used immunofluorescence and Western blots with antibodies that specifically recognize FAK phosphorylated on Y397 (pY397 FAK) in FAK-KO cells expressing either wtFAK or *FAK*^{K38AR86A} to disrupt its interaction with Arp2/3. Immunostaining and ratio imaging of pY397 FAK to total paxillin (Zaidel-Bar *et al.*, 2007) showed an overall increase in FAK phosphorylation at Y397 in FAK-KO cells reconstituted with *FAK*^{K38AR86A} compared with FAK-KO reconstituted with *wtFAK* (Figure 6A). Image segmentation and quantitative analysis confirmed this and showed that disruption of the FAK–Arp2/3 interaction with the FERM- domain mutant significantly increased levels of FAK Y397 phosphorylation in adhesions (Figure 6B). Western blot analysis of cell lysates showed that compared with FAK-KO cells reconstituted with *wtFAK*, FAK Y397 phosphorylation was significantly higher in FAK-KO cells reconstituted with *FAK*^{K38AR86A}, independently of whether cells were in suspension or plated for 60 min on FN (Figure 6C). Thus the FAK–Arp2/3 interaction decreases FAK Y397 phosphorylation in NA.

To determine whether Arp2/3 activity regulates FAK phosphorylation, we treated adherent cells with the Arp2/3 small-molecule inhibitor CK666 (100 µM for 60 min; Nolen *et al.*, 2009). Similar to genetic knockout of Arp2/3 subunits (Wu *et al.*, 2013), this treatment resulted in complete abolition of lamellipodia and NAs (unpublished data), precluding our ability to examine FAK phosphorylation in NAs by immunolocalization. However, Western blot analysis showed that Arp2/3 inhibition resulted in a substantial (20%) increase in FAK phosphorylation at Y397, indicating that Arp2/3 activity serves to temper FAK phosphorylation (Figure 6D). Together these results suggest that the FAK–Arp2/3 interaction might inhibit FAK activation in NAs.

We next tested whether the suppression of FAK activity by Arp2/3 binding was required for coupling lamellipodial protrusion and adhesion. This requirement would predict that inhibition of FAK activity would rescue the defects in leading edge behavior induced by disruption of the FAK–Arp2/3 interaction. We compared leading edge dynamics of FAK-KO cells expressing either wtFAK or *FAK*^{K38AR86A} and additionally treated with dimethyl sulfoxide (DMSO; control) or 1 µM FAK inhibitor PF573228 (Slack-Davis *et al.*, 2007). Examination of DIC movies and kymographs of the leading edge showed that the FAK inhibitor had little effect on leading edge behavior in FAK-KO cells expressing wtFAK (Figure 6E), similar to results in which FAK-KO was reconstituted with *FAK*^{Y397F} (Figure 3A). However, compared with FAK-KO cells expressing *FAK*^{K38AR86A}, which exhibited ruffling and lacked edge advance (Figure 4C), the leading edge behavior of FAK-KO cells expressing *FAK*^{K38AR86A} and additionally treated with FAK inhibitor was indistinguishable from that of either FAK-KO cells expressing wtFAK or *FAK*$^{+/+}$ controls (Figures 1A and 6E and Supplemental Movie S7). This was confirmed by quantitative analysis. Measurement of distances of protrusion and retraction showed that FAK inhibitor did not significantly change distances in FAK-KO cells expressing wtFAK, but the inhibitor did restore the difference between protrusion and retraction distances and velocities that was induced by disruption of the FAK–Arp2/3 interaction with *FAK*^{K38AR86A} (Figure 6, F and G). Restoration of the difference between protrusion and retraction distances by inhibition of FAK in cells with disrupted FAK–Arp2/3 interaction was sufficient to restore the protrusion efficiency and rescue the net edge advancement to levels similar to those of controls or FAK-KO cells expressing wtFAK (Figure 6, H and I). These results suggest that inhibition of FAK activity by Arp2/3 binding might be required for efficient leading edge advance.

To determine whether inactivation of FAK by Arp2/3 binding plays a role in regulating NA dynamics, we measured NA lifetime, formation density, and maturation fraction in FAK-KO cells expressing either wtFAK or *FAK*^{K38AR86A}, with or without the addition of 1 µM FAK inhibitor Pf573228 (Supplemental Movie S8). Quantitative analysis of TIRF movies of GFP-paxillin showed that pharmacological inhibition of FAK activity in FAK-KO cells reconstituted with wtFAK had little effect on NA lifetime or formation density but reduced the NA maturation fraction compared with DMSO control (Figure 7, J–L and N). In contrast, FAK inhibition in FAK-KO cells reconstituted with *FAK*^{K38AR86A} rescued the reduction in NA lifetime and increase in NA maturation fraction that was induced by disruption of the FAK–Arp2/3 interaction. However, the kinase inhibitor failed to rescue the decrease in NA formation density induced by disruption of the FAK–Arp2/3 interaction (Figure 6M). These results suggest that the inhibition of FAK by Arp2/3 binding is required for transient stabilization and subsequent turnover of NA and inhibition of their maturation, whereas the FAK–Arp2/3 interaction might promote dense NA formation independently of FAK kinase activity. Taken together, these results suggest that a major role of Arp2/3 binding is local inhibition of FAK activity in NA to couple lamellipodial protrusion to transient NA stabilization and turnover for efficient leading edge protrusion.

Haptosensing requires the FAK–Arp2/3 interaction, and mechanosensing during cell spreading requires FAK activation

To determine the physiological significance of NA–lamellipodia coupling through the FAK–Arp2/3 interaction, we assessed the ability of cells bearing perturbations in FAK activities to exhibit a haptic migratory response to ECM concentration or a mechanosensitive spreading response to ECM rigidity. It is well established that cells exhibit a biphasic migration velocity response to increasing concentrations of immobilized FN, with fastest velocities at intermediate FN concentrations (Palecek *et al.*, 1997; Gupton and Waterman-Storer, 2006). We first verified this biphasic haptic response in control cells by measuring migration speeds of cells plated at three different FN concentrations (1, 10, and 100 µg/ml) from time-lapse phase-contrast movies. This showed that cells plated on 10 µg/ml FN migrated significantly faster than cells on either 1 or 100 µg/ml FN, recapitulating previous results on other cell types (Figure 7A; Palecek *et al.*, 1997; Gupton and Waterman-Storer, 2006; Wu *et al.*, 2013). In FAK-KO cells, we found an overall reduction in migration speed at all FN concentrations compared with controls at the same concentration of FN. Comparison of speeds at different FN concentrations showed loss of biphasic behavior in FAK-KO cells, indicating that FAK is required for the haptic migration velocity response (Figure 7A). Expression of either wtFAK or the nonphosphorylatable mutant (FAK^{Y397F}) in FAK-KO cells rescued the biphasic curve, indicating that FAK's role in FN concentration sensing is independent of Y397 phosphorylation. In contrast, FAK-KO cells expressing the *FAK*^{K38AR86A} mutant migrated at the same speed, independent of FN concentration, indicating a loss of the biphasic velocity response. Thus the FAK–Arp2/3 interaction is required for the haptic migratory response to ECM concentration, but pY397 FAK is not.

We then determined the role of FAK activity and interaction with Arp2/3 in ECM stiffness mechanosensing. We assayed the ability of cells to spread when plated on ECMs of increasing rigidity. Cells were fixed after plating for 4 h on FN-coupled (10 µg/ml) compliant polyacrylamide substrates of 0.5, 1, 5, 10, 25, or 50 kPa and stained with phalloidin for determining cell area from wide-field epifluorescence images of actin. Quantification showed that, in general, cell

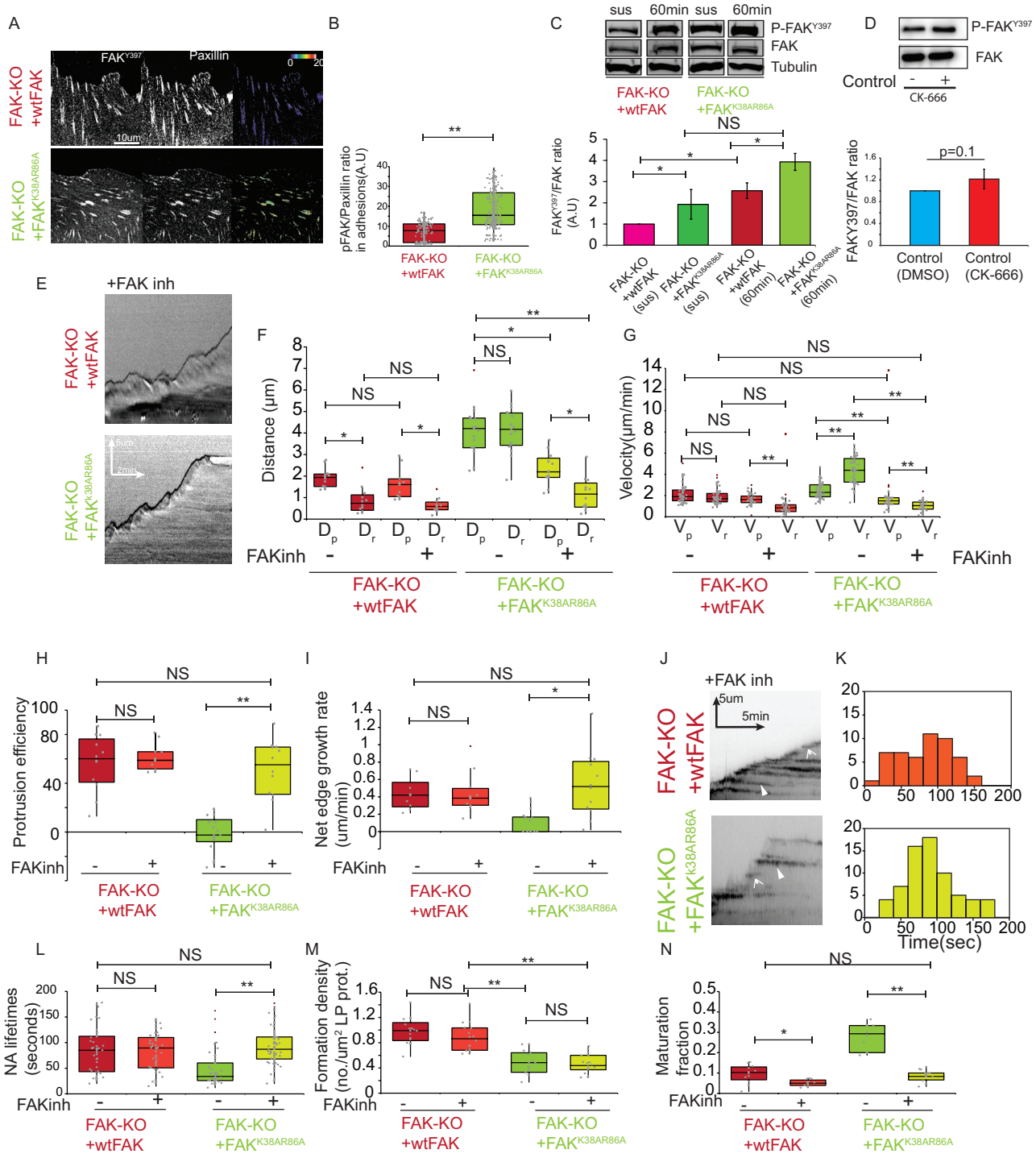

FIGURE 6: Arp2/3 sequesters inactive FAK to couple lamellipodial protrusion to transient NA stabilization and turnover for efficient leading edge protrusion. (A) Representative confocal micrographs of FAK$^{-/-}$ knockout (FAK-KO) cells expressing either mCherry-tagged wild-type FAK (FAK-KO + wtFAK; top) or mCherry-tagged FAK^{K38AR86A} (FAK-KO + FAK^{K38AR86A}) mutant immunostained for Y397 phosphorylation site–specific *FAK* antibody (P-FAK^{397}; left) and paxillin (middle). Right, fluorescence intensity ratio image of immunostained P-FAK^{397} to immunostained paxillin channels, color coded according to heat scale bar. Images were background subtracted and thresholded before ratio analysis. Magnification scale bar, 10 μm. (B) Box plot of fluorescence intensity ratio of immunostained P-FAK^{397} to immunostained paxillin in FAK-KO + wtFAK cells (red) or FAK-KO + FAK^{K38AR86A} cells (light green; 290–379 adhesions, five or six cells/condition). (C) FAK-KO + wtFAK cells (left) or FAK-KO + FAK^{K38AR86A} cells harvested at the time noted after plating on fibronectin and (top) Western blotted with antibodies to P-FAK^{397}, total FAK, and tubulin. Bottom, bar plot showing quantification of ratio of P-FAK^{397} to total FAK from three Western blots. (D) Control cells were plated on fibronectin for 4 h and treated with either DMSO (left lane, cyan bar) or 100 μM CK-666 (right lane, red bar) and (top) Western blotted with antibodies to P-FAK^{397} and total FAK. Bottom, quantification of ratio of P-FAK^{397} to total FAK from three Western blots. (E) Representative DIC kymographs of protrusion dynamics of FAK-KO + wtFAK (top) or FAK-KO + FAK^{K38AR86A}

spread area increased with increasing stiffness across all conditions. However, comparison between conditions showed that control cells spread the most on substrates of 25-kPa rigidity and either saturated or even slightly decreased cell area on 50-kPa substrates (Figure 7B). In contrast, FAK-KO cells showed only weak increase in cell area with increasing rigidity, with maximal spreading on 50-kPa substrates, indicating that FAK increases cells mechanosensitivity to ECM rigidity (Figure 7C). To describe the increase in cell spread area as a function of changes in ECM stiffness, we defined a parameter, "stiffness sensitivity" (μm^2/kPa), which is the maximum increase in cell spread area (A) divided by the difference in substrate rigidity (E) over which the area change occurs, $(A_{max} - A_{min})/(E_{max} - E_{min})$. This analysis showed that loss of FAK resulted in approximately threefold drop in stiffness sensitivity compared with control cells (Figure 7G). Expressing either wtFAK or the *FAK*^{K38AR86A} mutant in FAK-KO cells rescued the stiffness sensitivity of FAK-KO cells (Figure 7, D and F). In contrast, expression of FAK^{Y397F} in FAK-KO cells failed to rescue the defect, with cells bearing nonphosphorylatable FAK exhibiting stiffness sensitivity similar to FAK-KO cells (Figure 7E). Thus the mechanosensitive spreading response to ECM rigidity is phosphorylation dependent but independent of the FAK-Arp2/3 interaction. Taken together, these results show that FAK's roles in haptosensing and mechanosensing are mechanistically distinct: haptosensing requires the interaction of inactive FAK with Arp2/3, whereas mechanosensing during spreading is modulated by FAK activation.

DISCUSSION

We used quantitative high-resolution microscopy and specific perturbations to delineate the role of FAK in coupling lamellipodial protrusion to NA and determine the function of this coupling in cell behavior. We show that local and precisely timed regulation of FAK activity through its interaction with the lamellipodial actin nucleator Arp2/3 complex couples cell-edge protrusion to adhesion to mediate ECM sensing. Although the phenotype of FAK-KO cells has led to the well-accepted notion that FAK promotes disassembly of large FAs (Ilić *et al.*, 1995; Webb *et al.*, 2004; Ezratty *et al.*, 2005; Chan *et al.*, 2010), recent evidence indicates that FAK might also regulate NA in lamellipodia (Tilghman *et al.*, 2005; Owen *et al.*, 2007; Lawson *et al.*, 2012), although this had not been thoroughly examined. By analyzing FAK-KO cells, we find that FAK stabilizes lamellipodial dynamics to drive productive advance of the leading edge. This is achieved by FAK's promotion of the dense formation, transient stabilization, and subsequent timely turnover of NA within the lamellipodium and by inhibition of NA maturation into FA. We show that FAK activity is required for promoting the formation of a dense band of NA at the protruding cell edge, but FAK activity is dispensable for transient NA stabilization and leading edge advance, suggesting a critical role for inactive FAK in this process. Indeed, we show that FAK promotes localization of Arp2/3 to NA, where the FAK–Arp2/3 interaction may locally inhibit FAK activity to promote transient NA stabilization and productive leading edge protrusion. Unlike results with pure proteins in vitro (Serrels *et al.*, 2007), we find that the FAK–Arp2/3 interaction is not critical for enhancing actin polymerization in lamellipodia of living cells. Instead, using a FAK kinase inhibitor, we rescued defects in NA dynamics caused by disrupting the FAK–Arp2/3 interaction, further suggesting that local inhibition of FAK by Arp2/3 is critical for coupling NA turnover to lamellipodial protrusion. Taken together, these results highlight the precise spatiotemporal regulation of FAK activity that is required for coordinating protrusion with NA formation and turnover: FAK kinase activity contributes to the high density of NA formed as the lamellipodium protrudes and is critical for NA turnover and FA disassembly, whereas FAK interaction with Arp2/3 is vital for inhibiting FAK activity to delay their turnover long enough to couple lamellipodial actin treadmilling with leading edge advance.

Whereas *FAK*^{K38AR86A} has been shown to affect the direct interaction of FAK with the Arp2/3 complex with purified proteins in vitro as well as in cell extracts (Serrels *et al.*, 2007), the present study does not rule out the possibility that the effects of this mutant on leading edge and NA dynamics are due to changes in FAK interactions with other proteins besides Arp2/3 that might alter FAK's activity and downstream signaling. Previous studies showed that the FAK FERM domain is the site for many protein interactions with FAK, including p53, ezrin, and PIP2 (Frame *et al.*, 2010). In addition, the FERM domain is a critical regulator of FAK activity, as it can directly bind and inhibit the catalytic domain in-*trans* via two different sites, one in the F1 subdomain and the other in the F2 lobe (Cooper *et al.*, 2003; Lietha *et al.*, 2007). Thus mutations in the FERM domain may alter FAK activation and lead to downstream effects, including changes in FAK–Arp2/3 interaction and colocalization. Future studies will tease out whether activation of FAK and downstream signaling in NA is sufficient for loss of coupling between NA and the lamellipodial actin using phosphomimetic mutants of FAK such as FAK^{Y180AM183A} (Lietha *et al.*, 2007).

On the basis of our study and others, we suggest the following model for the organization and dynamics of the leading edge

(bottom) MEFs after 1-h treatment with 1 µM PF-228 (FAK inhibitor). Scale bar, distance 5 µm, time 2 min. (F) Box plot of distances (µm) of protrusion (D_p) and retraction (D_r) of FAK-KO cells expressing indicated cDNA with and without FAK inhibitor (FAKinh). Color coding in F–I and K–N: FAK-KO + wtFAK (no inhibitor, red; FAK inhibitor, orange), FAK-KO + FAK^{K38AR86A} (no inhibitor, light green; FAK inhibitor, yellow green; 10–12 cells/condition). (G) Box plot of velocities (µm/min) of protrusion (V_p) and retraction (V_r) of FAK-KO cells expressing indicated cDNA with and without FAK inhibitor (FAKinh; 10–12 cells/condition). (H) Box plot of protrusion efficiency (%) of FAK-KO + wtFAK and FAK-KO + FAK^{K38AR86A} cells with and without FAK inhibitor (10–12 cells/condition). (I) Box plot of net edge advance (µm/min) of FAK-KO + FAK and FAK-KO + FAK^{K38AR86A} cells with and without FAK inhibitor (10–12 cells/condition). $^{**}p < 0.0001$, $^{*}p < 0.005$; NS, not significant; Mann–Whitney *U* test. (J) Representative TIRF kymograph of eGFP-paxillin–marked adhesions in FAK-KO + wtFAK cells (top) or FAK-KO + FAK^{K38AR86A} cells (bottom) after treatment with FAK inhibitor. Scale bar, distance 5 µm, time 5 min. (K) Distribution of lifetimes of eGFP-paxillin marked NAs in FAK-KO + wtFAK cells (top) or FAK-KO + FAK^{K38AR86A} cells (bottom) after treatment with FAK inhibitor. (L) Box plots of quantification of NA lifetimes (seconds) from distributions in I. (M) Box plot of NA formation density (number/μm^2 lamellipodia protrusion area) marked by eGFP-paxillin in protruding lamellipodia of FAK-KO + wtFAK and FAK-KO + FAK^{K38AR86A} cells with and without FAK inhibitor (17–20 protrusions, five or six cells/condition). (N) Box plot for maturation fraction (dimensionless, NAs formed/NAs that mature) among >100 NAs in protruding lamellipodia of FAK-KO + wtFAK and FAK-KO + FAK^{K38AR86A} cells with and without FAK inhibitor (20 protrusions, five or six cells/condition). Note: FAK-KO + FAK and FAK-KO + FAK^{K38AR86A} data are the same as in corresponding plots of Figure 5. $^{**}p < 0.0001$, $^{*}p < 0.005$; NS, not significant; Mann–Whitney *U* test.

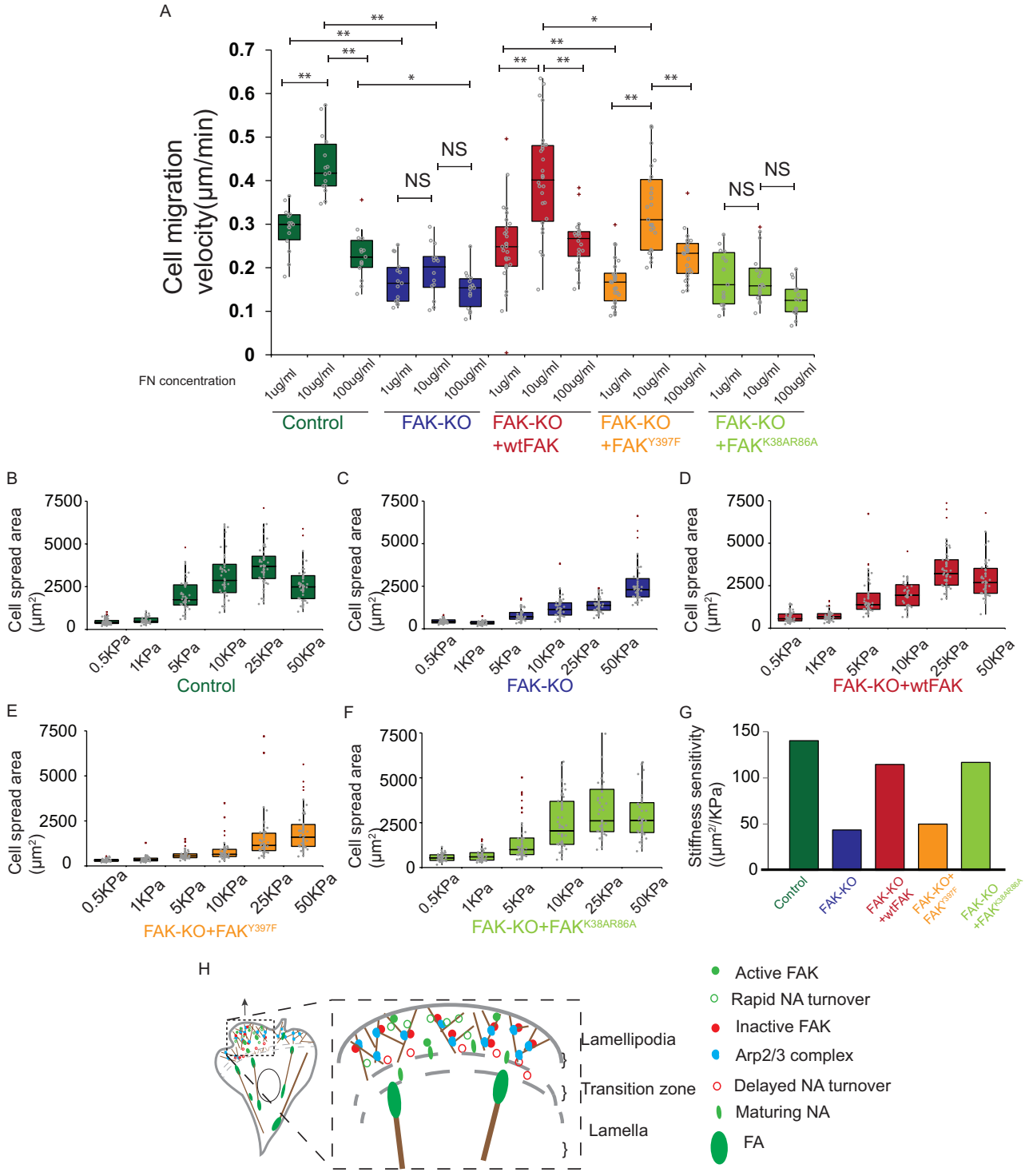

FIGURE 7: Haptosensing requires the FAK–Arp2/3 interaction, whereas mechanosensing during spreading requires FAK activation. (A) Box plot of random cell migration velocity (μm/min) determined from phase contrast movies (12 h; 10-min intervals) of indicated cells migrating on coverslips coated with different FN concentrations (1, 10, 100 μg/ml). Color coding in A–G: $FAK^{+/+}$ (control; dark green), $FAK^{-/-}$ knockout (FAK-KO; blue), FAK-KO cells expressing mCherry-tagged wild-type FAK (FAK-KO + wtFAK; red), eGFP-tagged FAK^{Y397F} mutant (FAK-KO + FAK^{Y397F}; yellow), or FAK-KO + mCherry-$FAK^{K38AR86A}$ mutant (FAK-KO + $FAK^{K38AR86A}$; light green; 15–30 cells/condition). (B–F) Box plots of cell spread area ($μm^2$) measured from epifluorescence images of Alexa 568–phalloidin staining of F-actin in fixed cells plated on FN-coupled polyacrylamide substrates of different stiffness (indicated in kPa; 50–95 cells/condition). (G) Bar plot of stiffness sensitivity ($μm^2$/kPa) defined as maximum increase in cell spread area divided by the difference in substrate rigidity over which the area change occurs for the indicated cells. $^{**}p < 0.0001$, $^{*}p < 0.005$; NS, not significant; Mann–Whitney *U* test. (H) Speculative model of the role of FAK in NAs based on our results and used for interpretation in the *Discussion*.

during cell migration (Figure 7H). A protrusion is formed by rapid polymerization of a polarized, dendritic actin network by the Arp2/3 complex (Pollard and Borisy, 2003). Arp2/3 localizes to the leading edge through mechanisms involving NPFs and small GTPase signaling (Higgs and Pollard, 2001; Ridley *et al.*, 2003) but independent of its interaction with FAK. As the protrusion forms, NAs are nucleated by actin-dependent activation and clustering of integrins within the lamellipodium (Alexandrova *et al.*, 2008; Choi *et al.*, 2008). NA formation may be mediated by integrin recruitment and activation in a preformed complex with kindlin (Bachir *et al.*, 2014) but could be facilitated by FAK activity (shown here) and FAK-mediated talin recruitment to cluster and further activate integrins (Lawson *et al.*, 2012). These pathways are not mutually exclusive. The high density of Arp2/3 in the lamellipodial actin network near NA may promote interaction of Arp2/3 and FAK in NA (Serrels *et al.*, 2007), mediating direct linkage between the branched actin network and NA. This interaction not only physically couples the lamellipodial actin network to ECM-bound integrins, but it also plays the role of transiently suppressing FAK activity. Inhibition of FAK activation in NA acts as a "time-delay relay," which stabilizes the protrusion by preventing the turnover of NA until after the dendritic array disassembles and Arp2/3 dissociates from the advancing lamellipodium. Thus the temporary inhibition of FAK activity in NA by either interaction with the Arp2/3 complex or through another mechanism that results in reduced association of FAK and the Arp2/3 complex promotes the perfect timing of NA turnover with lamellipodial actin treadmilling. The release of Arp2/3 by FAK that is facilitated by actin disassembly could allow reactivation of FAK, which could promote further integrin activation by FAK-mediated recruitment of talin, which could result in increased integrin-mediated FAK activation, which in turn could amplify the dissociation of FAK from Arp2/3 and NA from the branched actin network. Active FAK could then regulate its downstream targets such as RhoGEFs and other signaling proteins (Mitra *et al.*, 2005; Schaller, 2010) to start a feedback loop for the cycle to continue or promote signaling in adhesions that leads to mechanosensing and/or later FA disassembly.

We used haptosensing and mechanosensing assays to define the requirement for FAK activity and interaction with Arp2/3 in physiological functions. Remarkably, we found that FAK phosphorylation and FAK interaction with Arp2/3 mediate distinct cellular functions. Indeed, haptosensing of ECM concentration requires the interaction between FAK and Arp2/3, whereas FAK activation through Y397 phosphorylation modulates mechanosensing of ECM stiffness during spreading. These findings provide mechanistic insight into the notion that Arp2/3 is required for haptotaxis (Wu *et al.*, 2013) and indicate that precise coupling of protrusion with NAs that last the lifetime of the treadmilling actin array in lamellipodia optimize the ability of the lamellipodia to sense local gradients in ligands through the dense array of NAs. On the other hand, the requirement for FAK activity in sensitizing cells to ECM stiffness has been shown by others (Wang *et al.*, 2001) and could be mediated by functions of FAK in more mature FA through a paxillin phosphorylation pathway (Pasapera *et al.*, 2010; Plotnikov *et al.*, 2012).

In conclusion, we elucidate an important role for FAK in linking NA to the branched actin network through the Arp2/3 complex and an important role for this coupling in lamellipodial dynamics and ECM sensing during cell migration and spreading. We also show an important role for inactive FAK in NA in haptosensing. Combining our results with previous studies showing the role of FAK and FAK phosphorylation playing an important role in mechanosensing (Wang *et al.*, 2001), our results suggest a spatially and functionally distinct role for active and inactive FAK in NAs and FAs. We suggest that, like other kinases (Kholodenko, 2006), FAK is not just a binary switch but that the spatial and temporal dynamics of the level of FAK activation plays an important role in tuning different cellular functions.

MATERIALS AND METHODS

Cell culture

$FAK^{+/+}$ (control) and $FAK^{-/-}$ (FAK-KO) cells were a kind gift from D. D. Schlaepfer (University of California, San Diego, Moores Cancer Center, La Jolla, CA) and were maintained in DMEM supplemented with 10% fetal bovine serum (FBS; ThermoFisher, Waltham, MA) at 5% CO_2 and 37°C. For experiments, cells were plated at low confluency for at least 4 h on 22 × 22 mm #1.5 coverslips that had been coated with 10 µg/ml (unless otherwise noted) fibronectin (EMD Millipore, Billerica, MA) in PBS for 1 h at 37°C. All live-cell experiments were performed using phenol red–free DMEM containing 10% FBS, 20 mM 4-(2-hydroxyethyl)-1-piperazineethanesulfonic acid, and 10 U/ml Oxyrase (Oxyrase, Mansfield, OH) as imaging medium.

Reagents and transfection

cDNAs encoding eGFP- and mCherry-FAK, eGFP-actin, and mCherry- or mApple-paxillin were the kind gift of M. Davidson (Florida State University, Tallahassee, FL). eGFP-$FAK^{Y397F}$was a gift from D. D. Schlaepfer. Mouse embryonic fibroblasts (MEFs) were transiently transfected with 1 µg of DNA using Amaxa Kit V solution in an Amaxa Nucleofector (Lonza, Basel, Switzerland) with MEF alternate program T-020. Analysis of cell functions in FAK-KO cells that were rescued by reexpression of wild-type or mutant FAK constructs was carried out 36–48 h posttransfection. eGFP-actin imaging was done 4–12 h posttransfection, and all other experiments were done 24 h posttransfection. Cells were recovered in complete culture medium after transfection before plating on imaging coverslips. The FAK kinase inhibitor PF 573228 was purchased from Tocris Bioscience (Bristol, United kingdom) and used at 1 µM for 1–2 h. The Arp2/3 inhibitor CK 666 was purchased from Sigma-Aldrich and used at 100 µM for 1 h. Alexa 488–, 561–, and 655–phalloidin (1:400) was obtained from Invitrogen (ThermoFisher).

The following primary antibodies were used for indirect immunofluorescence (IF) and/or Western blots (WB): mouse anti-paxillin (IF 1:500; BD Biosciences, Franklin Lakes, NJ), mouse anti-FAK (clone 4.47; IF 1:50, WB 1:800; EMD Millipore), rabbit anti–p34-Arc/Arpc2 (IF 1:200; EMD Millipore), rabbit anti-phosphoFAK^{Y397} (31H5L17; IF 1:300, WB 1:2000; ThermoFisher), and rat anti-tubulin (DM1A; WB 1:5000; Sigma-Aldrich, St. Louis, MO).

The previously published Arp3 subunit-binding, double point mutant of FAK, $FAK^{K38AR86A}$ (Serrels *et al.*, 2007), was constructed via site-directed mutagenesis of eGFP-FAK using QuikChange II (Agilent Technologies, Santa Clara, CA) and verified by sequencing. The following primers were used:

K38A primer 1: 5′-GGGGCCATGGAGCGAGTCCTAGCGGTTTTTCACTACTTTGAAAACAGCAGC-3′.

K38A primer 2: 5′- GCTGCTGTTTTCAAAGTAGTGAAAAACCGCTAGGACTCGCTCCATGGCCCC-3′.

R86A primer 1: 5′- TGTGGCCTGCTATGGGTTGGCACTCAGTCATCTGCAGTCTGAGGAGG-3′.

R86A primer 2: 5′-CCTCCTCAGACTGCAGATGACTGAGtgcCAACCCATAGCAGGCCACA-3′.

Western blot

Cells lysed in Laemmli sample buffer were separated by SDS–PAGE and electro-transferred to Immobilon-F. Membranes were blocked with 5% nonfat dry milk (or 3% bovine serum albumin [BSA]) in TBS-T buffer (20 mM Tris, pH 7.6, 137 mM $NaCl_2$, 0.1% [vol/vol] Tween-20) incubated with primary antibody overnight at 4°C, washed with TBS-T, and incubated with appropriate fluorescent secondary antibodies (IRDye 680RD and IRDye 800CW; Li-Cor), and bands were resolved with an Odyssey scanner (Li-Cor). Quantification of Western blots was performed using MetaMorph software (Molecular Devices, Sunnyvale, CA) using integrated intensity measurements after background subtraction.

Microscopy

High-resolution DIC microscopy for all cell types was conducted on an inverted microscope system (TE2000E; Nikon, Melville, NY) using a 60× Plan Apo 1.40 numerical aperture (NA) objective lens and 1.4 NA oil condenser. Illumination was provided by an LED source (Lumencor, Beaverton, OR) and attenuated with heat-cut and 546-nm band-pass filters. Illumination was timed with image acquisition by an electronic shutter (Sutter Instruments, Novato, CA), and stage position was controlled by an automated stage (Applied Scientific Instrumentation, Eugene, OR). Images were acquired every 3 s. The same system was also used with a 20× Plan Ph 0.45 NA objective and a phase-contrast condenser for long-term time-lapse imaging of cells plated on 1, 10, and 100 µg/ml of fibronectin using multistage acquisition mode. Images were taken every 10 min for 12 h. TIRF microscopy of eGFP-paxillin in control, FAK-KO, FAK-KO + mCherry-FAK, FAK-KO + $FAK^{K38AR86A}$, or mApple-paxillin with either EGFP-FAK or EGFP-FAK^{Y397F} was performed on an inverted TIRF microscope system (TiE; Nikon) using a 100×/1.49 NA Apo TIRF objective lens. Illumination was provided by a 150-mW, 488-nm or 150-mW, 546-nm laser (Coherent, Santa Clara, CA) in a custom-designed laser combiner (Spectral Applied Research, Richmond Hill, ON). Illumination was delivered to the TIRF illuminator (Nikon) by a single-mode optical fiber (Oz Optics). Stage position was controlled with an automated stage fitted with a piezo top plate (Applied Scientific Instrumentation). Pairs of images were captured every 3 or 5 s. Spinning-disk confocal (SDC)–fluorescent speckle microscopy of eGFP-actin or mApple-actin was performed on an inverted microscope system (TiE-Nikon) fitted with a CSU-X1 confocal scanner (Yokogawa, Musashino, Japan) using a 100×/1.49 NA Plan Apo objective lens. Illumination was provided by a 500-mW, 488-nm (Coherent) or 1000-mW, 561-nm laser (MPB Communications, Pointe-Claire, Quebec, Canada) in a custom-designed laser combiner (Spectral Applied Research, Canada). Illumination was delivered to the confocal scanner by a single-mode optical fiber (Oz Optics). Stage position was controlled with an automated stage fitted with a piezo top plate (Applied Scientific Instrumentation, Eugene, OR). Images were captured at the same frame rate of 3 s. Immunofluorescence micrographs of paxillin, actin, FAK^{Y397}, FAK, and the ArpC2 subunit of the Arp2/3 complex were acquired by SDC on the microscope described, using a 100×/1.49 Plan Apo TIRF objective. All microscopes were controlled using MetaMorph software. Temperature was maintained at 37°C (airstream incubator; Nevtek, Williamsville, VA), and images were acquired using a cooled charge-coupled device (CoolSNAP-HQ2 or CoolSNAP MYO; Photometrics, Tucson, AZ).

Immunofluorescence

Indirect immunofluorescence was performed as described (Pasapera *et al.*, 2010). Briefly, cells on coverslips were fixed with 4% paraformaldehyde in cytoskeleton buffer (CB; 10 mM 2-(*N*-morpholino)ethanesulfonic acid, pH 6.1, 138 mM KCl, 3 mM MgCl, 2 mM EGTA) for 30 min at 37°C and then permeabilized for 5 min with 0.25% Triton X-100 in CB. Free aldehydes were reacted with 10 mM glycine, and coverslips were washed in TBS and blocked in blocking solution (2% BSA immunoglobulin-free and protease-free in TBS-T; Sigma-Aldrich). Cells were incubated with indicated antibodies diluted in blocking solution overnight and then washed and incubated with fluorophore-conjugated secondary antibodies and fluorophore-conjugated phalloidin for 1 h. Subsequent to wash, coverslips were mounted on slides with mounting medium (Pathology Products; Dako, Carpinteria, CA).

Mechanosensing assay

Glass-bottom six-well plates containing flexible substrates of different stiffnesses (0.5, 1, 5, 10, 25, and 50 KPa) were obtained from Matrigen Life Technologies (Brea, CA). Wells were washed and coated with 10 µg/ml fibronectin for 1 h at 37°C, and indicated cells were plated and allowed to spread for 4 h before fixation. Subsequent to fixation and extraction as described, cells were incubated with either Alexa 488– or Alexa 561–phalloidin for 1 h. Cells were then washed with TBS-T and then mounted with TBS.

Image analysis

All images were analyzed using MetaMorph software, except for colocalization analysis, which was done with Fiji (http://fiji.sc/Fiji) using the JACoP plug-in (Bolte and Cordelieres, 2006), as described in what follows.

Leading edge dynamics. Kymographs for cell protrusion and retraction dynamics from DIC movies were carried out as previously described (Giannone *et al.*, 2004). Quantities describing leading edge dynamics were obtained from kymographs by calculating the slope and length of each protrusion and retraction. Frequency was obtained by manually counting number of cycles of protrusion and retraction in a kymograph. Net edge advance was calculated by measuring the distance between the start of the first protrusion at the beginning of the kymograph to the end of the last retraction in the kymograph.

FA size distribution. SDC images of paxillin immunofluorescence were first low-pass filtered (filter size 3×3 pixels) and then manually thresholded, binarized, and morphologically filtered ("open close"; 2-pixel kernel). The segmented area of thresholded regions was then determined (MetaMorph).

NA formation density. Formation densities were obtained as previously described (Thievessen *et al.*, 2013). TIRF image sequences of cells expressing EGFP-paxillin, EGFP-FAK, or EGFP-FAKY397F during protrusion formation were analyzed by hand to count the number of newly assembling NAs. Diffraction-limited intensity maxima that were stable for >10 s were counted as NAs, and shorter NAs were excluded. The leading edge in the region was outlined in each frame and to normalize the number of NAs to the lamellipodial area gained.

NA maturation fraction. Maturation fractions were obtained using TIRF image sequences of cells expressing eGFP-paxillin, EGFP-FAK, or EGFP-FAK^{Y397F} during protrusion formation (Thievessen *et al.*, 2013). NAs in protruding lamellipodia were manually counted in a protrusion and in subsequent image sequences, NAs that matured to FAs were manually counted (MetaMorph). Maturation fraction was reported as the fraction of NAs that matured to FAs relative to the initial number of NA.

NA lifetimes. NA lifetimes were reported from TIRF image sequences of cells expressing eGFP-paxillin, EGFP-FAK, or EGFP-FAKY397F during protrusion formation (Thievessen *et al.*, 2013). Image sequences were low-pass filtered before analysis. Kymographs were generated using a 1-pixel-wide line drawn perpendicular to the leading edge. Length of eGFP-tagged protein streaks in kymographs was measured in the time domain of the kymograph. NAs were identified as diffraction limited spots with a lifetime between 10 and 200 s. Only NAs that nucleated and turned over during the course of the movie were selected for analysis, and the rest were excluded. All NA analysis was done in MetaMorph.

Distance between the lamellipodium and NA. SDC images of mCherry-FAK constructs and immunostained ArpC2 subunit were background-subtracted and low-pass filtered. A 10-pixel-wide line was drawn perpendicular to the leading edge, and the average fluorescence intensities of the two channels were obtained. The distance between the lamellipodium and NA was reported as the distance between the peaks of the ArpC2 channel and the FAK channel.

Colocalization analysis. Colocalization analysis for FAK and Arp2/3 were carried out in Fiji software using the JACoP plug-in (Bolte and Cordelieres, 2006). SDC images were background-subtracted using the rolling ball algorithm in FIJI. Regions were drawn along the lamellipodia in the Arp2/3 complex channel or FAK channel and transferred to the corresponding FAK channel or Arp2/3 complex channel. ROIs were extracted, and the plug-in was used to obtain the Manders colocalization parameters.

Actin dynamics. SDC-FSM image sequences of eGFP-actin or mApple-actin were low-pass filtered, and kymographs were obtained from 1-pixel-wide lines drawn perpendicular to the leading edge. Slopes of actin flow streaks were used to obtain retrograde flow velocities. Slope of protrusion was used to calculate protrusion velocities, and the two quantities were summed to get the polymerization rate.

pFAK^{Y397}/paxillin immunofluorescence image ratio. SDC images were background-subtracted by using background images with the same image acquisition settings as for cell images. Adhesions were thresholded as described, and Image arithmetic (MetaMorph) was used to generate ratio images of phosphoFAK/paxillin. Image morphometry was then used to extract ratio values for each adhesion and repeated.

Cell area. Cells were stained with fluorescent phalloidin, images were manually outlined (MetaMorph), and the segmented area was determined.

Cell migration velocity. Nuclei were manually tracked using the Track Points function (MetaMorph), and instantaneous velocities (between consecutive frames) were determined and averaged for each cell.

Statistical analysis

All data were analyzed using Excel (Microsoft) with the Analyze-it tool. Nonnormally distributed data were analyzed using the Mann–Whitney *U* test. Box plots were used for data representation, with the bottom and top of the box representing the first and third quartiles, respectively, and the band in the box representing the median. Outliers are shown as red asterisks.

ACKNOWLEDGMENTS

We thank Dave Schlaepfer for the kind gift of FAK$^{-/-}$ and FAK$^{+/+}$ fibroblasts, members of the Waterman Lab for helpful discussion, Bill Shin for maintenance of the microscopes, and Schwanna Thacker for administrative assistance. This work was supported by the Division of Intramural Research, National Heart, Lung and Blood Institute, National Institutes of Health.

REFERENCES

Alexandrova AY, Arnold K, Schaub S, Vasiliev JM, Meister JJ, Bershadsky AD, Verkhovsky AB (2008). Comparative dynamics of retrograde actin flow and focal adhesions: Formation of nascent adhesions triggers transition from fast to slow flow. PLoS One 3, e3234.

Bachir AI, Zareno J, Moissoglu K, Plow EF, Gratton E, Horwitz AR (2014). Integrin-associated complexes form hierarchically with variable stoichiometry in nascent adhesions. Curr Biol 24, 1845–1853.

Bear JE, Svitkina TM, Krause M, Schafer DA, Loureiro JJ, Strasser GA, Maly IV, Chaga OY, Cooper JA, Borisy GG, *et al.* (2002). Antagonism between Ena/VASP proteins and actin filament capping regulates fibroblast motility. Cell 109, 509–521.

Bolte S, Cordelieres FP (2006). A guided tour into subcellular colocalisation analysis in light microscopy. J Microsc 224, 13–232.

Burnette DT, Manley S, Sengupta P, Sougrat R, Davidson MW, Kachar B, Lippincott-Schwartz J (2011). A role for actin arcs in the leading-edge advance of migrating cells. Nat Cell Biol 13, 371–381.

Chan KT, Bennin DA, Huttenlocher A (2010). Regulation of adhesion dynamics by calpain-mediated proteolysis of focal adhesion kinase (FAK). J Biol Chem 285, 11418–11426.

Choi CK, Vicente-Manzanares M, Zareno J, Whitmore LA, Mogilner A, Horwitz AR (2008). Actin and alpha-actinin orchestrate the assembly and maturation of nascent adhesions in a myosin II motor-independent manner. Nat Cell Biol 10, 1039–1050.

Choi CK, Zareno J, Digman MA, Gratton E, Horwitz AR (2011). Cross-correlated fluctuation analysis reveals phosphorylation-regulated paxillin-fak complexes in nascent adhesions. Biophys J 100, 583–592.

Cooper LA, Shen T-L, Guan J-L (2003). Regulation of focal adhesion kinase by its amino-terminal domain through an autoinhibitory interaction. Mol Cell Biol 23, 8030–8041.

Ezratty EJ, Partridge MA, Gundersen GG (2005). Microtubule-induced focal adhesion disassembly is mediated by dynamin and focal adhesion kinase. Nat Cell Biol 7, 581–590.

Frame MC, Patel H, Serrels B, Lietha D, Eck MJ (2010). The FERM domain: organizing the structure and function of FAK. Nat Rev Mol Cell Biol 11, 802–814.

Giannone G, Dubin-Thaler BJ, Döbereiner HG, Kieffer N, Bresnick AR, Sheetz MP (2004). Periodic lamellipodial contractions correlate with rearward actin waves. Cell 116, 431–443.

Gupton SL, Waterman-Storer CM (2006). Spatiotemporal feedback between actomyosin and focal-adhesion systems optimizes rapid cell migration. Cell 125, 1361–1374.

Hamadi A, Bouali M, Dontenwill M, Stoeckel H, Takeda K, Rondé P (2005). Regulation of focal adhesion dynamics and disassembly by phosphorylation of FAK at tyrosine 397. J Cell Sci 118, 4415–4425.

Higgs HN, Pollard TD (2001). Regulation of actin filament network formation through ARP2/3 complex: activation by a diverse array of proteins. Annu Rev Biochem 70, 649–676.

Hoffmann JE, Fermin Y, Stricker RL, Ickstadt K, Zamir E (2014). Symmetric exchange of multi-protein building blocks between stationary focal adhesions and the cytosol. Elife 2014, 1–18.

Ilić D, Furuta Y, Kanazawa S, Takeda N, Sobue K, Nakatsuji N, Nomura S, Fujimoto J, Okada M, Yamamoto T (1995). Reduced cell motility and enhanced focal adhesion contact formation in cells from FAK-deficient mice. Nature 377, 539–544.

Iskratsch T, Yu CH, Mathur A, Liu S, Stévenin V, Dwyer J, Hone J, Ehler E, Sheetz M (2013). FHOD1 is needed for directed forces and adhesion maturation during cell spreading and migration. Dev Cell 27, 545–559.

Kholodenko BN (2006). Cell-signalling dynamics in time and space. Nat Rev Mol Cell Biol 7, 165–176.

Lauffenburger DA, Horwitz AF (1996). Cell migration: a physically integrated molecular process. Cell 84, 359–369.

Lawson C, Lim ST, Uryu S, Chen XL, Calderwood DA, Schlaepfer DD (2012). FAK promotes recruitment of talin to nascent adhesions to control cell motility. J Cell Biol 196, 223–232.
Lietha D, Cai X, Ceccarelli DFJ, Li Y, Schaller MD, Eck MJ (2007). Structural basis for the autoinhibition of focal adhesion kinase. Cell 129, 1177–1187.
Machacek M, Hodgson L, Welch C, Elliott H, Pertz O, Nalbant P, Abell A, Johnson GL, Hahn KM, Danuser G (2009). Coordination of Rho GTPase activities during cell protrusion. Nature 461, 99–103.
Mitra SK, Hanson DA, Schlaepfer DD (2005). Focal adhesion kinase: in command and control of cell motility. Nat Rev Mol Cell Biol 6, 56–68.
Mullins RD, Heuser JA, Pollard TD (1998). The interaction of Arp2/3 complex with actin: nucleation, high affinity pointed end capping, and formation of branching networks of filaments. Proc Natl Acad Sci USA 95, 6181–6186.
Nolen BJ, Tomasevic N, Russell A, Pierce DW, Jia Z, McCormick CD, Hartman J, Sakowicz R, Pollard TD (2009). Characterization of two classes of small molecule inhibitors of Arp2/3 complex. Nature 460, 1031–1034.
Owen KA, Pixley FJ, Thomas KS, Vicente-Manzanares M, Ray BJ, Horwitz AF, Parsons JT, Beggs HE, Stanley ER, Bouton AH (2007). Regulation of lamellipodial persistence, adhesion turnover, and motility in macrophages by focal adhesion kinase. J Cell Biol 179, 1275–1287.
Palecek SP, Loftus JC, Ginsberg MH, Lauffenburger DA, Horwitz AF (1997). Integrin-ligand binding properties govern cell migration speed through cell-substratum adhesiveness. Nature 385, 537–540.
Pasapera AM, Schneider IC, Rericha E, Schlaepfer DD, Waterman CM (2010). Myosin II activity regulates vinculin recruitment to focal adhesions through FAK-mediated paxillin phosphorylation. J Cell Biol 188, 877–890.
Plotnikov SV, Pasapera AM, Sabass B, Waterman CM (2012). Force fluctuations within focal adhesions mediate ECM-rigidity sensing to guide directed cell migration. Cell 151, 1513–1527.
Pollard TD, Borisy GG (2003). Cellular motility driven by assembly and disassembly of actin filaments. Cell 112, 453–465.
Ponti A, Machacek M, Gupton SL, Waterman-Storer CM, Danuser G (2004). Two distinct actin networks drive the protrusion of migrating cells. Science 305, 1782–1786.
Renkawitz J, Schumann K, Weber M, Lämmermann T, Pflicke H, Piel M, Polleux J, Spatz JP, Sixt M (2009). Adaptive force transmission in amoeboid cell migration. Nat Cell Biol 11, 1438–1443.
Ridley AJ, Schwartz MA, Burridge K, Firtel RA, Ginsberg MH, Borisy G, Parsons JT, Horwitz AR (2003). Cell migration: integrating signals from front to back. Science 302, 1704–1709.
Schaller MD (2010). Cellular functions of FAK kinases: insight into molecular mechanisms and novel functions. J Cell Sci 123, 1007–1013.
Schneider IC, Hays CK, Waterman CM (2009). Epidermal growth factor-induced contraction regulates paxillin phosphorylation to temporally separate traction generation from de-adhesion. Mol Biol Cell 20, 3155–3167.
Serrels B, Serrels A, Brunton VG, Holt M, McLean GW, Gray CH, Jones GE, Frame MC (2007). Focal adhesion kinase controls actin assembly via a FERM-mediated interaction with the Arp2/3 complex. Nat Cell Biol 9, 1046–1056.
Slack-Davis JK, Martin KH, Tilghman RW, Iwanicki M, Ung EJ, Autry C, Luzzio MJ, Cooper B, Kath JC, Roberts WG, *et al*. (2007). Cellular characterization of a novel focal adhesion kinase inhibitor. J Biol Chem 282, 14845–14852.
Thievessen I, Thompson PM, Berlemont S, Plevock KM, Plotnikov SV, Zemljic-Harpf A, Ross RS, Davidson MW, Danuser G, Campbell SL, *et al*. (2013). Vinculin-actin interaction couples actin retrograde flow to focal adhesions, but is dispensable for focal adhesion growth. J Cell Biol 202, 163–177.
Tilghman RW, Slack-Davis JK, Sergina N, Martin KH, Iwanicki M, Hershey ED, Beggs HE, Reichardt LF, Parsons JT (2005). Focal adhesion kinase is required for the spatial organization of the leading edge in migrating cells. J Cell Sci 118, 2613–2623.
Tomar A, Lawson C, Ghassemian M, Schlaepfer DD (2012). Cortactin as a target for FAK in the regulation of focal adhesion dynamics. PLoS One 7, e44041.
Vallotton P, Ponti A, Waterman-Storer CM, Salmon ED, Danuser G (2003). Recovery, visualization, and analysis of actin and tubulin polymer flow in live cells: a fluorescent speckle microscopy study. Biophys J 85, 1289–1306.
Wang HB, Dembo M, Hanks SK, Wang Y (2001). Focal adhesion kinase is involved in mechanosensing during fibroblast migration. Proc Natl Acad Sci USA 98, 11295–11300.
Webb DJ, Donais K, Whitmore LA, Thomas SM, Turner CE, Parsons JT, Horwitz AF (2004). FAK-Src signalling through paxillin, ERK and MLCK regulates adhesion disassembly. Nat Cell Biol 6, 154–161.
Welch MD, Mallavarapu A, Rosenblatt J, Mitchison TJ (1997). Actin dynamics in vivo. Curr Opin Cell Biol 9, 54–61.
Wu C, Haynes EM, Asokan SB, Simon JM, Sharpless NE, Baldwin AS, Davis IJ, Johnson GL, Bear JE (2013). Loss of Arp2/3 induces an NF-κB-dependent, nonautonomous effect on chemotactic signaling. J Cell Biol 203, 907–916.
Wu X, Suetsugu S, Cooper LA, Takenawa T, Guan J-L (2004). Focal adhesion kinase regulation of N-WASP subcellular localization and function. J Biol Chem 279, 9565–9576.
Zaidel-Bar R, Milo R, Kam Z, Geiger B (2007). A paxillin tyrosine phosphorylation switch regulates the assembly and form of cell-matrix adhesions. J Cell Sci 120, 137–148.